Time-lapse approach to correct deficiencies of 2D soil zymography

Andrey Guber[a*], Evgenia Blagodatskaya[c], Archana Juyal[a], Bahar S. Razavi[b], Yakov Kuzyakov[d,e,f], Alexandra Kravchenko[a],

[a] *Department of Soil, Plant and Microbial Sciences, Michigan State University, East Lansing, MI, USA*

[b] *Department of Soil and Plant Microbiome, University of Kiel, Kiel, Germany*

[c] *Department of Soil Ecology, Helmholtz Centre for Environmental Research – UFZ, Halle (Saale), Germany*

[d] *Department of Soil Science of Temperate Ecosystems, University of Goettingen, Goettingen, Germany*

[e] *RUDN University, Moscow, Russia*

[f] *Institute of Physicochemical and Biological Problems in Soil Science, Russian Academy of Sciences, 142290 Pushchino, Russia*

* Corresponding author: A.K. Guber. E-mail: akguber@msu.edu. 1066 Bogue st., East Lansing, MI, 48824, USA

Highlights

- Soil zymography ignores product diffusion and underestimates enzyme activity.
- New time-lapse zymography (TLZ) accounted for diffusion losses.
- TLZ produces realistic assessments of spatial soil enzyme activity.

ABSTRACT

Membrane zymography is commonly used in rhizosphere ecology for mapping enzyme activities in intact soil samples and plant roots. The method consists of incubating a membrane saturated with an enzyme-specific fluorogenic substrate on the soil/root surface followed by measurements of fluorescence intensity of the product in the membrane. The traditional zymography is based on assumptions that fluorescence on membrane images is linearly increasing with time during zymography and an increase in product content is numerically equal to enzyme activity in soil

below the membrane. These assumptions are unlikely to hold in experimental settings. Here we introduce a new zymography technique, *time-lapse zymography (TLZ)*; the approach that eliminates the need for assumptions of the traditional zymography and provides more realistic estimates of enzymatic activities. We assessed the new technique in a series of laboratory and modeling experiments, including quantification of the fluorescent product diffusion (e.g. MUF: 4-methylumbelliferone) from plant roots, enzyme activity measurements on the roots, and HYDRUS-2D & HP2 software calibration with obtained data. The calibrated model was used to analyze the processes governing spatial and temporal dynamics of MUF contents in the membrane. The results indicated that the enzyme diffusion within the membrane-soil system was negligible, and measured zymograms were adequately reproduced solely by accounting for substrate and product diffusions and for catalytic enzyme reaction described by the Michaelis-Menten equation. TLZ enabled identifying and using linear parts on MUF time series and accounting for MUF losses in each zymogram pixel, considerably improving the accuracy as compared to the traditional method. Results demonstrated that enzymatic activity from only a thin soil layer (~ 0.2 mm) is adequately represented in zymograms.

Keywords: Soil enzyme activity, HYDRUS-2D & HP2 software, enzyme diffusion, plant roots, switchgrass, maize.

Abbreviations: MUF, 4-methylumbelliferon; RMSE, the Root-Mean-Square Error; NSE, the Nash–Sutcliffe model efficiency coefficient; TLZ, time-lapse zymography.

1. INTRODUCTION

Current challenge to visualize and co-localize soil and rhizosphere biochemical processes call for methodology enabling adequate interpretation and quantification of images. Membrane-based imaging that initially used a filter paper soaked in substrate (Dinkelaker and Marschner, 1992) to visualize and quantify *in situ* enzymatic activity, was intensively developed during past decades by employing an imprinting technique on nitrocellulose membranes (Grierson and Comerford, 2000), application of substrate mixed with fluorogenic or colorimetric reagents (Dong et al., 2007) and suggesting a *2D soil zymography* protocol for *in situ* mapping of enzyme activities (Jones et al., 2011). The membrane-fluorometric approach, was further modified by combinations with agarose gel (Baldrian and Větrovský, 2012; Spohn et al., 2013; Giles et al., 2018) or by direct attachment of membrane to the soil surface (Sanaullah et al., 2016) that

enhanced quality and resolution of images. It is widely applied nowadays to intact soil and roots to quantify acid phosphatase, aminopeptidase, chitinase, and β-glucosidase activities (Spohn and Kuzyakov 2013, 2014; Guhr et al., 2015; Hoang et al., 2016; Razavi et al., 2016; 2017; Ge et al., 2017; Liu et al., 2017; Ma et al., 2017, 2018; Heitkotter and Marschner 2018; Wei et al., 2019; Hummel et al., 2021). The membrane-fluorometric approach is particularly useful in: (i) analysis at high resolution of the spatial distribution of enzyme activities and functionality jointly produced in soil by the plant, fungal, and bacterial communities (Dong et al., 2007; Zhang et al., 2020), and (ii) monitoring the development of enzymatic processes in space and time by repeated measurements avoiding destructive sampling.

During zymography a membrane saturated with an enzyme-specific fluorogenic substrate is placed on the surface of a soil/root sample for essentially long time (up to several hours). Upon a contact of the substrate with soil enzymes, a fluorescent product (e.g. 4-methylumbelliferon (MUF), or 7-amido-4-methylcoumarin (AMC)) is released and its presence on the membrane is detected in the UV light. The fluorescing pattern on the membrane (zymogram) reflects the spatial distribution of active enzymes on the soil surface. Calculations of the enzymatic activity at zymograms are based on the following assumptions: (i) the substrate concentration in the membrane is sufficient to maintain a constant catalytic rate of the enzymes during zymography; (ii) the catalytic reaction starts immediately upon the membrane's contact with the soil/root surface; (iii) the fluorescence on membrane images is linearly increasing with time during zymography; and (iv) the increase of fluorescence in the membrane is numerically equal to enzyme activity on the soil/root surface. With these assumptions the rate of enzymatic reaction can be calculated by simply dividing the product content in the membrane measured at the end of the membrane incubation on the soil surface by the duration of incubation. The product content in the membrane is calculated from brightness of the fluorogenic product on zymography images using calibration (Guber at al., 2019).

The listed above assumptions behind enzymatic activity calculations are never tested in practice, despite the fact that fluorescence-based membrane zymography demonstrated non-linear increase in the grayscale value over incubation time (Fig. 1a in Dong et al., (2007)). At best, published works mention that incubation times were estimated based on preliminary studies, however, the details on such preliminary studies are rarely provided. Despite significant

progress in 2D soil zymography several methodological issues still hinder interpretation of zymographic results.

The first issue is the lack of standardized zymography procedure. The settings for the incubation experiments are far from being standardized. The experiment durations can range widely from 20-30 minutes (Dong et al., 2007; Jones et al., 2011) to one hour (Sanaullah et al., 2016; Razavi et al., 2016), or even 4-18 hours (Spohn et al., 2013) for membranes attached to a thick (1 mm) agarose gel (Spohn and Kuzyakov, 2014). Concentrations of substrates used in zymography experiments can also vary by several order of magnitude (e.g. from as low as 10 μM (Razavi et al., 2017) to as high as 12 mM (Spohn and Kuzyakov, 2014)) to match the activity in specific soils (Jones et al., 2011; Razavi et al., 2019). Different zymography settings make the results of zymography incomparable.

The second issue that complicates interpretation of zymographic results is the possibility of enzyme movement, including enzyme diffusion through the gel in gel-based zymography (Spohn and Kuzyakov 2013, 2014) or Brownian motion of enzymes in the soil pore solution in membrane-based zymography (Holz et al., 2019). If enzyme diffusion takes place, then the number of reactive enzyme molecules, the catalytic reaction time and rates vary temporally and spatially during zymography, violating the assumption of constant catalytic rate of the enzymes in space and time and reducing accuracy of the activity calculations.

The third issue is appearance of spots in the membrane with brightness exceeding sensitivity of the camera light sensor (e.g. charge coupled device (CCD)) during zymography. Enzymatic activity varies greatly among enzymes of different origin and micro-environmental conditions even within relatively small soil volume. This leads to high spatial variability in the production rates of fluorogenic agents and requires much shorter membrane incubation durations for the zones with high enzymatic activity as compared to those with low activity. This problem can be illustrated by an analogy with photographing objects under contrasting light conditions, where bright objects appear overexposed, while dark objects underexposed on the photos. Excessive incubation of zymography membranes results in zones with high enzymatic activity to become oversaturated by the fluorogenic product, when increase in the product content in the membrane in time does not increase proportionally membrane brightness. Due to only minor changes in brightness with further increasing content of the product in the oversaturated zones the assumption of the linear relationship between the fluorescence and the product content in the

membrane becomes invalid, resulting in essential underestimation of enzymatic activity (Guber et al., 2019).

The last, but not least issue is omnidirectional diffusion of the product from enzyme active sites in the soil during the incubation experiments. It was shown (Dong et al., 2007) that considerable amounts of the 4-methylumbelliferone residue remained in the soil 8 days after *in situ* soil zymography. The diffusion complicates interpretation of soil zymograms and introduce the uncertainty in calculations of enzymatic activity (Guber et al., 2018). It is generally unknown how much of the total product catalyzed by enzymes is detected by the membrane and how long it takes the product to approach the membrane. Very rough estimates showed that enzyme activities detected via 2D zymography represent only a ~20% of the actual enzymatic reactions that take place within a thin soil layer directly contacting zymography membrane (Guber et al., 2018). This hinders the ability to recalculate the surface-measured enzyme activities into the gravimetric of volumetric units.

The goals of this study were: (i) to critically examine the traditional *in situ* soil zymography with an emphasis on the physical processes occurring in the soil and in the membrane during soil zymography; and (ii) to propose a new approach to 2D zymography implementation in order to alleviate the impact of the above-mentioned issues and to improve the accuracy of enzymatic activity calculations. The specific objectives were: (i) to examine the dynamics of MUF appearance in the membrane sections associated with and/or free of enzymes; (ii) to introduce the time-lapse approach to zymography measurements; (iii) to use the new approach for testing the assumptions employed in the 2D soil zymography; (iv) to quantify and account for the diffusion of the substrate and product while processing soil zymograms.

2. Materials and Methods

The whole study consisted of two laboratory and two modeling experiments. We first introduced a new zymography technique, which enables measurements of MUF content dynamics in individual pixels of zymography membrane and building on these dynamics in calculations of the enzyme activity. Then, in the *MUF diffusion experiment*, we examined MUF diffusion from roots without soil to the membrane in the absence of substrate and enzymatic reaction. In the *Root zymography experiment* the substrate was added to the membrane to trigger enzymatic reaction in order to study the diffusion of released MUF to the membrane. Then, the diffusion of substrate, the enzymatic reaction and the diffusion of MUF were modeled to

reproduce the results of the *Root zymography experiment* with the goal to calibrate the model and assess the effect of diffusion on estimates of enzymatic activities measured by 2D membrane zymography. Finally, the calibrated model was used to analyze and correct the impact of distance between the membrane and enzymes on the estimates of the enzyme activity.

2.1 Time-lapse zymography

Here we introduce a new zymography technique, which is based on the time-lapse photography principle, and thus referred further to as *time-lapse zymography (TLZ)*. The key difference of the proposed technique from the traditional zymography is in using a sequence of images taken during membrane incubation on the soil surface. Thus, in the time-lapse approach the activity is derived from the information on the dynamics of the product appearances in the membrane's pixels during incubation. In this sense we propose a nearly continuous zymography contrary to a single-image traditional technique.

2.1.1 Experimental setup and procedure

The experimental setup for the time-lapse soil zymography includes a Canon EOS Rebel T6 camera with a Canon EF 75-300 mm f/4-5.6 III Telephoto Zoom Lens (Canon U.S.A., Inc.) connected via a 7 mm extension tube ring (Fotodiox, Inc. USA) to reduce the focusing distance of the lens (Fig. S1a). The camera is mounted on a Rocwing Pro Copy Stand 145 (Rocwing Co., UK). A 22W Blue Fluorescent Circline Lamp - FC8T9/BLB/RS (Damar Worldwide 4 LLC) is used as a source of UV light. Helicon remote software (Helicon Soft Ltd., Ukraine) allows the time-lapse imaging with remote camera settings, automatically acquiring images and transferring them from camera to PC at desired time intervals (Fig. S1b. The camera settings, i.e. the aperture of f/5.6, exposure time of 1/125 sec and ISO speed ratings of 3200, were defined experimentally (Guber et al., 2019).

The setup is designed for soil core and rhizobox zymography (Fig. S1c) with a hydrophilic polyamide membrane filter of 100 μm thickness with average pore size of 0.45 μm (Tao Yuan, China). The membrane is saturated in 6 mM solution of 4-methylumbelliferone-β-D-glucopyranoside (referred further to as the substrate), covered by a transparent not-reflecting light film, and fixed in the zymography frame (Fig. S1d). The film prevents evaporation of the substrate from the membrane and convective transport of the product (MUF) due to the gradient of matrix pressure between the soil and the drying membrane. The substrate concentration was estimated from results of preliminary experiments and of the modeling study as such that is

necessary to support enzyme activity at levels not limited by substrate, avoid stimulation of microorganisms in soil to produce new enzymes, and produce MUF in amounts detectable during 1-hour membrane zymography (Guber et al., 2018, 2019). The soil and roots surfaces are slightly prewetted by misting a DI water over the rhizobox to bring soil-membrane interface close to saturation and thus ensure good hydraulic contact between the soil surface and zymographic membrane. Oversaturation can potentially enhance convection transport of the substrate and reduce MUF diffusion from soil to membrane due to water flow from the soil-membrane interface into the soil, and thus must be avoided. Then, the frame with the membrane is placed on the soil surface and incubated for 45-60 minutes in the dark. The incubation time for specific enzymes and soil may differ and should be estimated in the preliminary trials. Four low compression springs installed in the corners of the frame keep the membrane in contact with the soil and roots, while preventing soil compaction during zymography (Fig. S1d). The photos are taken under the UV light every minute automatically during the whole incubation period. The same setup and settings are used for the membrane calibration with the standard MUF solutions (Guber et al., 2018). The calibration parameters (Supplemental materials S1) were used to convert zymograms to MUF concentrations.

2.1.2 Image processing

Every zymography generated from 45 to 60 images (zymograms) with pixel sizes of 15 x 15 μm. The total number of images varied depending on the zymography duration and provided a nearly continuous (every minute) record of the fluorescence development in the membranes. A multi-step procedure was developed for processing TLZ (Supplemental materials).

2.2 Soil and root materials used in the experiments

Undisturbed soil cores were used to compare the traditional zymography with TLZ. Six cores 5 × 5 cm (ID × height) were taken from 5-10 cm depth in the field under long-term monoculture switchgrass (*Panicum virgatum* L.) (var. Southlow) in Marshall farm of Great Lakes Bioenergy Research Center, Kellogg Biological Station, southwest Michigan, USA (85°24″ W, 42°24″ N). The soil was fine loamy, mixed, mesic Typic Hapludalf (Kalamazoo series) developed on a glacial outwash. Soil texture was sandy loam (59% sand, 34% silt, and 7% clay). Upon collection, three of the cores were planted with switchgrass seeds and upon germination 2-3 switchgrass plants were grown in the cores for 6 weeks, while the other three cores were not

planted, but watered as the planted cores. After switchgrass termination, the cores were wrapped with foil and kept for 8 months at 4 °C for the slow decomposition of roots.

Roots of young maize (*Zea mays* L.) plants (3-weeks after germination) were used in the diffusion and zymography experiments. The plants were grown in rhizoboxes in a greenhouse. The roots, separated from the soil, were rinsed in DI water to remove soil particles, and kept air dry at 20 ºC for two months to suppress microbial activity. The activity of β-glucosidase in maize roots remained high during at least 4 months of storing in these conditions. In preliminary study β-glucosidase activity in maize roots was 21.8±5.3, 18.0±7.3 and 13.4±4.4 pmol min^{-1} mm^{-2} after 60, 90 and 120 days of air-drying, respectively.

2.3 MUF diffusion experiment

The MUF diffusion experiment was conducted to assess the fraction of the total MUF cleaved by the enzymes from substrate that could be detected during 2D zymography. In the previous study we demonstrated that during zymography only small fraction (< 20%) of MUF diffused from the soil surface to the membrane (Guber et al., 2018). In this study we analyzed the diffusion of MUF to the membrane from plant roots without soil. For that, instead of saturating the membrane with the enzyme-specific substrate solution, as is done in standard 2D zymography measurements, we saturated the root fragments with MUF solution. Then we covered the roots with MUF-free membrane and recorded the development of fluorescence signal in the membrane due to MUF diffusion from the roots.

Two fragments of maize roots 12 to 15 mm long and approximately 0.4 mm in diameter (Fig. 1a) were soaked in 6 mM MUF solution for 10 minutes and placed on the acrylic surface of an empty rhizobox. The roots were slightly prewetted by misting a DI water to ensure good hydraulic contact between their surface and the membrane. A zymography membrane saturated in 0.1 M MES-buffer solution was inserted into the frame, covered by a transparent film, and fixed on the root surface. The membrane was subjected to TLZ for 30 minutes as described in Section 2.1.1. The TLZ images were processed as described in Section S2 of Supplemental materials, and greyscale values (G) of individual pixels were converted to MUF contents [pmol mm^{-2}] using the equation obtained in the calibration experiment:

$$MUF_i^j = 0.0254 \cdot G_i^j \quad (1)$$

where superscript j denotes time [min], and subscript i denotes pixel in the image.

MUF diffusion was analyzed in six 2.25 mm cross-sections drawn perpendicular to each root (Fig. 1 b). Root thicknesses in the cross-sections were equal to 0.418 ± 0.036 mm and 0.423 ± 0.025 mm for the *root-A* and *root-B*, respectively. The vertical projection of roots on the membrane of size of the root thickness is referred further to as the root-associated area. MUF distributions were calculated along the cross-sections in the root-associated areas and beyond them using "Plot Profile" tool of Imagej/Fiji software (Schindelin et al., 2012). To quantify MUF diffusion beyond the root-associated area, we calculated the distances from the root centers along the membrane that encompass 50%, 75% and 90% of the total MUF detected for each time interval. In addition to the cross-sections, we analyzed MUF time series measured at 0, 0.4 and 0.6 mm distances from the centers of the root-associated area.

2.4 Root zymography experiment

The root zymography experiment was conducted to estimate the *β*-glucosidase activity on the root surfaces. Four root fragments were soaked in DI water for 10 minutes (Fig. 1c) and subjected to the TLZ. Unlike the *MUF diffusion experiment*, here the membrane was saturated in 6 mM solution of 4-methylumbelliferone-*β*-D-glucopyranoside, referred further to as the *substrate*. The membrane was fixed on the root surface and subject to the TLZ for 90 minutes with a time interval of 1 minute. Longer zymography time was chosen due to imperfect contact between the roots and membrane surfaces in the absence of soil, which results in large substrate and product (MUF) diffusion lengths and travel time.

MUF distributions were analyzed in 2.25 mm cross-sections drawn perpendicular to each root (Fig. 1d). Fine root tips (0.22 mm and 0.24 mm thick) were selected for these measurements to minimize the effects of root thickness and spatial variability of enzymatic activity on the roots on MUF distributions in the membranes. For comparison with the *MUF diffusion experiment*, we analyzed MUF time series measured in the locations within the membranes corresponding to the root centers and at distances of 0.4 mm and 0.6 mm from the root centers.

2.5 Modeling of soil zymography

The goal of the modeling was to better understand the processes involved in the 2D zymography and correctly interpret its results. Similar to the previous study (Guber et al., 2018) we used HYDRUS-2D coupled with HP2 software (Šimůnek et al., 2012), which simulates two-dimensional transport and transformation of multiple chemicals in a variably-saturated porous

media. The HP2 component of software allows introducing user-defined bio-chemical reactions without modification of HYDRUS-2D code. This model is typically used at scales larger than the size of soil pores, however the size of mesh elements and diffusion equations solved in HYDRUS-2D are valid for the scale of soil zymography.

2.5.1 Modeling the root zymography experiments

Mathematically, soil zymography is a three-dimensional solute transport problem; hence, its modeling is computationally expensive. However, the elongated shape of roots selected for modeling allowed us to simplify the simulation domain and to solve a two-dimensional (2D) problem for each root cross-section (Fig. 1d). Therefore, the modeled system consisted of the substrate-saturated membrane, the plant root with enzymes on its surface, and water films on the root and membrane boundaries. The 2D modeled domain (1.05 mm length × 0.30 mm height) represented a fragment of the substrate-saturated membrane placed over the root (Fig. 2). The thickness of the membrane was 0.1 mm. Due to axial symmetry only one half of the root cross-section area was simulated. The domain length estimated from the root zymography was set so as to eliminate the effect of the right boundary (Block 8 in Fig.2) of the domain on MUF concentration. Therefore, measured and modeled changes in MUF content in Block 8, located at the greatest distance from the root, were negligible. The first block of the membrane corresponding to the root associated zone, was 0.1 mm long, while the lengths of the other seven blocks (Blocks 2-8) corresponding to the MUF diffusion zone were 0.15 mm each. Therefore, each block corresponded to 10 pixels on zymography images.

Due to saturated conditions, and zero water fluxes at boundaries of the domain, water flow, and convection transports of the substrate and product were neglected in simulations. We modeled substrate diffusion from the substrate-saturated membrane to water surrounding the root, substrate cleavage by enzymes on the root surface, and omnidirectional diffusion of produced MUF from the root surface to water and membrane. In preliminary microplate enzyme assays for different soils we observed linear increase of signal with time during 2-hours incubation in a wide range of substrate concentrations. These results indicated that either enzymes are not produced and not decayed during the assay, or the production compensated for the decay. Enzyme diffusion was not observed in previous zymography study (Guber at al., 2018). Therefore, enzyme production, decay and diffusion were not considered in zymography modeling. The substrate diffusion, driven by gradients of concentration between the substrate-

saturated membrane and initially substrate-free water, resulted in continuously changing substrate concentrations on the root surface. To account for the variable concentration in MUF production, the Michaelis-Menten equation (Michaelis and Menten, 1913; Johnson and Goody, 2011) was introduced to the HP2 code:

$$\frac{dP}{dt} = \frac{V_{max}S}{K_m+S} \quad (2)$$

where P and S are concentrations of the product (MUF) and substrate in the liquid phase, respectively [μmol ml^{-1} solution]; V_{max} is the maximum rate of enzymatic activity [μmol min^{-1} ml^{-1} solution]; K_m is the half saturation constant [μmol ml^{-1} solution]; and t is time (min).

Note, since catalysis of the substrate occurred in the solution surrounding the roots, in the model, all parameters of the Michaelis-Menten equation were expressed in mass units of solution volume. This differs from the traditional enzyme assays presenting V_{max} in mass units of soil mass [μmol min^{-1} g soil^{-1}]. Strictly speaking, enzymatic reactions in enzyme-kinetics assays occur in soil suspensions, rather than in a bulk soil. Therefore, both P and S concentrations are attributed to the liquid phase. Since enzymes are associated with the solid phase (i.e. roots, soil particles) a unit conversion from [ml solution] to [g dry soil/root] through soil dilution rates [g dry soil/root ml^{-1} solution] is commonly used for the product and parameters in the enzyme assays. The units based on the solution volume are more convenient for modeling. For example, in modeling decomposition of soil organics by extracellular enzymes the parameters V_{max} and K_m are expressed in soil volume units (Allison et al., 2010; German et al., 2012), which can easily be converted either to soil mass or liquid volume units using soil bulk density and water content.

To mimic the experimental conditions of the *Root zymography experiment*, we set up the initial pressure heads corresponding to a water equilibrium state across the simulation domain with 0 cm head at the lowest point (Z = -0.2 mm). Therefore, both substrate and product diffusions occurred at nearly saturated water contents. All fluxes were set to zero at the domain boundaries. The initial conditions for the chemical substances were set as: V_{max} = 0, P = 0, S = 6 μmol ml^{-1} in the membrane, V_{max} = 0, P = 0, S = 0 in the water and inside the roots, and P = 0, S = 0 on the root surface. The parameter K_m for β-glucosidase on the root surface was set equal to 0.0271 μmol ml^{-1} (German et al., 2012). The unknown model parameter V_{max} on the root surface was fitted to the dynamics of MUF content measured in the *Root zymography experiment.* The spatial distribution of the enzyme density and activity on the root surface is generally unknown,

and it was deemed impractical to fit V_{max} values within each node of the root-surface (Fig. 2, yellow nodes). Therefore, we used a single V_{max} for all root-surface nodes, assuming that it represented a spatially averaged value representative of the whole root surface.

To fit HYDRUS-2D & HP2 to the experimental data measured in the *Root zymography experiment* we varied V_{max} in Eq.(2) until the best agreement between the modeled and measured MUF contents was achieved. As the HP2 version of HYDRUS-2D software does not support automatic fitting, nor batch mode, the V_{max} was searched for manually using the Golden-section algorithm (Press et al., 2007). We used the cumulative MUF mass per unit of membrane width [pmol mm^{-1}] measured in the first six blocks (Fig. 2) at one-minute interval during the first 30 minutes of the experiment to estimate V_{max}.

The model performance was assessed using the Root-Mean-Square Error (RMSE) and the Nash–Sutcliffe model efficiency coefficient (NSE):

$$RMSE = \sqrt{\sum_{i=1}^{n}\left(MUF_o^i - MUF_m^i\right)^2/n}$$

$$NSE = 1 - \frac{\sum_{i=1}^{n}\left(MUF_o^i - MUF_m^i\right)^2}{\sum_{i=1}^{n}\left(MUF_o^i - \overline{MUF_o}\right)^2} \quad (3)$$

where MUF_o^i is the MUF mass in each block measured at time i [pmol mm^{-1}], MUF_m^i is the modeled MUF mass for the same time moments [pmol mm^{-1}], $\overline{MUF_o}$ is the time-averaged MUF mass in each block [pmol mm^{-1}], n=30 is the number of time moments in observations. NSE = 1 indicates a perfect match of modeled MUF contents to the observed values, while NSE = 0 means that the model predictions are as accurate as the mean of the observed data. The range 0.5 < NSE < 0.65 is considered as acceptable for model performance in hydrology (Ritter and Muñoz-Carpena, 2013; Moriasi et al., 2013). The objective functions for the fitting procedure were minimum RMSEs and Maximum NSEs in the first 6 blocks of the membrane.

The calibrated model was used to calculate the percentages of total MUF released by enzymes that appeared in the whole membrane and in the root-associated zones, as well as to calculate the dynamics of enzymatic activities in the course of root zymography:

$$v_i^t = \frac{1}{A_r}\frac{dP_i^t}{dt} \quad (4)$$

where v_i^t is the actual enzymatic activity per unit of root-associated area of the membrane at time t [pmol min^{-1} mm^{-2}], A_r is the root-associated area of the membrane in the XY-plane (root

width) [mm^2], P_i^t is the MUF content at time *t* [pmol], the subscript *i* denotes the whole system ($i = 0$) or the number of block in the membrane (Fig. 2a, Block 1 – Block 8).

2.5.2 *Modeling case study: the effect of the enzyme position on soil zymography results*

The calibrated HYDRUS-2D & HP2 model was applied to analysis of the impact of distance between the membrane and enzymes on the estimates of the enzyme activity obtained from the membrane zymography. We assumed that, due to diffusion losses, MUF contents detected in the membrane decreased nonlinearly with this distance and caused increasing underestimation of enzymatic activity.

The same simulation domain (Fig. 2), modeled processes, initial and boundary conditions (Section *2.5.1*) were used in the next set of simulations. Five simulation scenarios reflecting different root positions below the membrane were explored, specifically with root distance from the membrane being set to 0.0, 0.05, 0.10, 0.15, and 0.20 mm. To account for the potential effect of V_{max} on the activity detected in the membrane, we ran the five simulation scenarios in V_{max} range slightly wider than that obtained during model calibration (i.e. 10, 60 and 100 nmol min^{-1} ml^{-1}). The results of simulations were presented as the activity v_i^t time series separately for the whole system and each of 8 blocks of the membrane to calculate maximum enzymatic activities $\max(v_i^t)$ and time t_p, when the maxima were achieved for each modeling scenario. These maxima are referred further as peak activities. The percentage of detected activity $v_{\%}^d$ was calculated in each block of the membrane as:

$$v_{\%}^d = 100 \cdot \max(v_i^t)/\max(v_0^t) \tag{5}$$

where $\max(v_i^t)$ and $\max(v_0^t)$ are the peak activities calculated in the membrane blocks and the total system, respectively (Fig. 2).

To quantify the effect of the peak activity time on $v_{\%}^d$ and the time, when $v_{\%}^d$ drops by 50% we fitted a non-linear regression equation to the relationship between $v_{\%}^d$ and t_p obtained for the root-associated zone:

$$\begin{gathered} v_{\%}^d = a + \frac{b}{c+t_p}; \qquad 1 \le t_p \le t_p^{max} \\ t_{50} = 2b/\left(\frac{b}{c+1} - a\right) - c \end{gathered} \tag{6}$$

where t_p is the peak activity time [min], t_p^{max} is the maximum peak activity time obtained in the simulations.

2.6 Processing root and soil core zymograms

The zymograms measured at the undisturbed soil cores (Sections 2.1) and roots (Sections 2.4) were processed using the traditional and TLZ approaches. For the traditional approach the activity was calculated as the MUF content in the membrane detected on the 30th minute of the experiment divided by the zymography duration (i.e., by 30 min).

For TLZ, the maximum peak activities, $\max(v_i^t)$, and the peak activity time, t_i^p, were calculated individually for each pixel as described in Supplemental materials. Then, the peak activities in the image pixels, $\max(v_i^t)$, were corrected for the detection losses associated with the MUF diffusion as:

$$\begin{aligned} v_i^0 &= f_i \max(v_i^t) \\ f_i &= 100/\left(a + \frac{b}{c + t_i^p}\right) \end{aligned} \tag{7}$$

where v_i^0 are the corrected peak activities in the image pixels [pmol min^{-1} mm^{-2}], f_i is the correction factor calculated in each image pixel using the fitted parameters of Eq.(6).

Finally, we analyzed the time series of the total numbers of pixels with non-zero activities and selected the upper and lower thresholds on the t_p images based on the shape of the curves. Binarized t_p images were used as a mask for the v_i^0 images to exclude the noise and artifacts from the activity images.

3 Results

3.1 MUF diffusion experiment

No fluorescent or dark spots were observed in the zero-time zymogram. This indicated that MUF in the roots was invisible through the membrane, the membrane was MUF-free, and the quenching effect of roots was negligible (images not shown).

The brightness of zymograms increased over time in the membrane at areas of close proximity to the roots. MUF contents calculated from zymograms along the six root cross-sections (Fig. 1b) increased gradually over time, with the highest values located in the center of the roots and declining rapidly to the root peripheries (Fig. 3a,b). Approximately 50% of MUF

detected in the membrane was within the root area at all time moments. The areas encompassing 75% and 90% of the observed MUF increased over time for the *root-2a* (Fig. 3a) and remained relatively constant for the *root-2b* (Fig. 3b). On average, 75% of the MUF mass was located within 0.35 mm and 0.39 mm, and 90% of the mass within 0.51 mm and 0.59 mm zones around the root 2a and 2b, respectively.

The results of the *MUF diffusion experiment* suggest that, independent of time, considerable amounts of the MUF (*ca* 50%) that approached the membrane during 2D soil zymography diffuse beyond areas of active enzymes, and thus contribute to diffusion MUF losses within the membrane.

3.2 Root zymography experiment

The shapes of MUF distributions along the root cross-sections obtained in the *Root zymography experiment* (Fig. 3c and 3d) resembled those of the *MUF diffusion experiment* (Fig. 3a and 3b). Approximately 50% of MUF mass was located within the root centers, and 75% and 90% of MUF mass encompassed nearly the same areas around the roots as in the *MUF diffusion experiment.* However, the tailing part of the distributions was less pronounced in this experiment compared to the *MUF diffusion experiment.* The total MUF mass detected on the membrane for the *root-2a* (Fig. 3c) was approximately twice that for the *root-2b* (Fig. 3d), indicating either higher enzymatic activity in the *root-2a* or shorter distance between this root and membrane, and thus, larger amount of MUF reached the membrane during zymography from this root as compared to those from *root-2b*.

The time series of MUF content in the *Root zymography experiment* differed from those in the *MUF diffusion experiment* (Fig. 4b). The shapes of the MUF vs. time curves were similar in both experiments only for the root-associated areas of the *root-2a* (Fig. 4a red and black circles, Fig. 4b black circles). For the *root-2b* there was a lag time in the MUF arrival to the membrane, which increased with the distance from the root along the membrane (Fig. 4b, red symbols). Moreover, the concave shape of the MUF curves at distances 0 and 0.4 mm changed to a convex shape for the 0.6 mm distance from the centers of both roots.

Similar to the *MUF diffusion experiment,* the large differences between the MUF contents of the two roots observed in the root centers, substantially decreased at 0.4 mm distance from the roots and almost disappeared at the 0.6 mm distance (Fig. 4b).

In summary, the *Root zymography experiment* confirmed that MUF distribution on the membrane during soil zymography is largely driven by diffusion. The results revealed an existence of a lag time in the MUF temporal dynamics measured at different distances from the roots.

3.3 Modeling the Root zymography experiment

The HYDRUS-2D & HP2 model reproduced the experimental data of the *Root zymography experiment* reasonably well (Fig. 5). Root-mean-square errors of simulated MUF contents were 0.145 ± 0.042 and 0.136 ± 0.092 pmol mm^{-1} for the *root-2a* and *root-2b*, respectively. The NSE values were 0.979 ± 0.014 and 0.890 ± 0.187 for the same roots (Table 1). Low RMSE values, and the NSE values close to 1 (except for the *root-2b*, block 6) indicated an acceptable model accuracy in reproducing MUF content in the membrane. It is worth mentioning that the adequate model fits were obtained only after the vertical distance between the membrane and the root surface was set to 0.08 and 0.19 mm for the *root-2a* and *root-2b*, respectively.

The model adequately reproduced the shapes of the MUF dynamics in different sections of the membranes (Fig. 5). Surprisingly, the differences in the shapes and absolute values of MUF contents between the two roots did not translate into large differences in the values of V_{max} parameters of the HYDRUS & HP model, which were equal to 67 nmol min^{-1} ml^{-1} for the *root-2a* and 62 nmol min^{-1} ml^{-1} for the *root-2b*.

The dynamics of MUF contents in the membrane expressed as the percentage of the total MUF mass in the modeled system also differed between the two roots. The percentage of the total MUF in the membrane increased faster and was greater for the same time moments for the *root-2a* than for the *root*-2b (Fig. 6a, green lines). Overall, ~19% and 16% of the total MUF produced in the system was recovered in the membranes during the 90-min experiments for the *root-2a* and *root-2b*, respectively. The percentages of the recovered MUF were much smaller (2.8% and 2.5%) for the root-associated areas of the membranes (Fig. 6a, red lines). Here, the recovery was the highest (3.8%) on the 20^{th} minute of the experiment for the *root-2a*, and then decreased. For the *root-2b* the maximum recovery (2.6%) occurred only on the 33^{rd} minute of the experiment.

The differences in the MUF content dynamics measured in the membranes for the two roots translated into the differences in the calculated enzymatic activities for the whole system and for the root-associated areas on the membranes (Fig. 6b). The activities estimated from the total

MUF contents in the system peaked 7 minutes earlier and were twice as large for the *root-2a* as compared to *root-2b*, (Fig. 6b, black lines). The activities estimated for the same roots based on the MUF contents in the root-associated zones of membranes peaked 14 minutes earlier and were 3 times larger, respectively (Fig. 6b, red lines). Therefore, there were both time and rate discrepancies in assessment of enzymatic activities using MUF contents in the whole system and root-associated areas of membranes.

3.4 Modeling case study: the effect of the enzyme position on soil zymography results

An overall increase in the time of peak activities with the root distance from the membrane was observed for the root-associated section of the membrane and the whole system in HYDRUS-2D & HP2 simulations. This increase was close to linear for the whole system (Fig. 7a, closed symbols) and non-linear for the root-associated area of the membrane (Fig. 7a, open symbols). At zero distance between the root and the membrane the $\underline{t_p}$ values were smaller for the root-associated area as compared to the whole system. However, the slope of $\underline{t_p}$ curves was much steeper for the root-associated area than that for the whole system resulting in larger $\underline{t_p}$ values for the root-associated areas at a distance of 0.2 mm (Fig. 7a).

Unlike $\underline{t_p}$, the peak activity, max(v^t), decreased with the distance between the root and the membrane. This decrease was linear for the whole system (Fig. 7b, closed symbols). For the root-associated area of the membrane, the max(v^t) values decreased fast when the distance increased from zero to 0.05 mm, but then remained almost constant for the distances > 0.15 mm (Fig. 7b, open symbols).

The $\underline{t_p}$ and max(v^t) trends and their absolute values were affected by the maximum rate of enzymatic activity V_{max}. The slope of $\underline{t_p}$ curves gentled and the $\underline{t_p}$ values decreased, while inverse trends occurred for max(v^t) curves as V_{max} increased from 10 to 100 pmol min^{-1} mm^{-2} indicating a faster response of the system to the substrate addition at larger V_{max} (Fig. 7a,b). Consistently with this observation, the detected activity $v_{\%}^{d}$ calculated by Eq.(5) also increased with increasing V_{max} (Fig. 7c), though $v_{\%}^{d}$ decreased exponentially with the distance between the root and the membrane for all V_{max} (Fig. 7c). The effect of V_{max} on $v_{\%}^{d}$ almost disappeared for $\underline{t_p}$ > 1 min when the detected activity was plotted vs. the time of the peak activity (Fig. 7d). This curve was accurately approximated (R^2 = 0.93) by Eq.(6) with the parameter values a = 2.95, b = 26.0 and c = 0.84 in the range of 1 < $\underline{t_p}$ < 45 min. The errors of approximation were relatively high only for

the zero-distance scenario (t_D > 1 min), that is in the case of a perfect contact between the root and the membrane. It should be noted that in the membrane soil zymography the perfect contact rarely occurs (Guber et al., 2018).

3.5 Comparing traditional and time-lapse zymography approaches

Traditional processing of single zymography images, by dividing MUF content in pixels by zymography duration (30 min), generated S-shaped histograms (in a log-scale) with predominance of low activity (Fig. 8, top row, closed symbols). Contrary to the traditional approach, all histograms for the TLZ had a bell-shape, skewed toward low activity with the peak around 0.4 pmol min^{-1} mm^{-2} and overall greater number of pixels with high activity (Fig. 8, top row, open symbols). These histograms changed quite a bit after multiplying max(v^t) by the correction factor *f*. The histograms gained left inclining limbs and smoothed, their activity increased by a factor of 24, and their shapes became closer to log-normal distribution in all experiments (Fig. 8, bottom row).

The differences between the two zymography approaches are well pronounced in the enzymatic activity maps calculated for the *Root zymography experiment* and soil cores from the control (no plants) and switchgrass treatments (Fig. 9). The traditional activity images are rather blurred with a lot of spots with low activity between the roots (Fig. 9a). The TLZ images are more contrasted with fewer low activity pixels between enzyme-active spots (Fig. 9 b,e,h). However, the diffusion front, well visible around the roots (Fig. 9b), remained in these images. Correcting the activity for the MUF losses resulted in an overall increase of activity in the pixels, removal of large part of the diffusion front and improvement of image sharpness (Fig. 9, c,f,i).

4 DISCUSSION

4.1 MUF diffusion experiment

Two important implications can be drawn from the analysis of the MUF distribution patterns on zymography membranes from the plant root originated MUF (Fig. 3). The first implication is that, due to diffusion, a substantial amount of MUF from the source, i.e., roots in this experiment, is lost on the way to the recipient, i.e., the membrane. Three MUF diffusion components considered here (Fig. 10) are: (1) diffusion from the root to the root-associated zone in the membrane (blue arrows); (2) lateral diffusion within the membrane (green arrows); and (3) radial diffusion (red arrows), that is, an omnidirectional diffusion of MUF from the root.

Assuming, negligible diffusion inside the root, the first and the third diffusion components add up to the total MUF production in the system.

In the traditional membrane zymography the enzymatic activity is calculated based on the (1), (2), and partly (3) diffusion components. The results of the *MUF diffusion experiment* suggest a relocation of MUF that has already reached the membrane from the root-associated zone of the membrane to the MUF diffusion zone due to the lateral diffusion. MUF also reaches the diffusion zone by diffusing radially from the root. Despite known MUF contents in both root-associated and diffusion zones, the contributions of the lateral and radial diffusions to the MUF patterns on the membrane (Fig. 3) are impossible to separate from each other, because they are constantly changing over time. It is equally impossible to assess their individual effects on calculations of the enzymatic activity in more complex systems, than that used in the *MUF diffusion experiment*, due to overlapping MUF diffusion fronts originated from multiple enzyme spots located in close proximity to each other. Our results indicate that underestimation of the enzymatic activity by traditional zymography must be at least 50% in a case of a perfect contact of enzymes with the membrane and increase with increasing distance between enzymes and the membrane simply due to MUF losses for radial diffusion (Fig. 3).

The second implication is that a substantial portion of MUF (~ 50%) detected on the membrane at any time point is located beyond the area associated with the MUF source. A gradual decrease of MUF content in the membrane with distance from the roots, typically observed on zymograms of plant roots taken within the soil, suggests presence of spatial patterns in enzymatic activity. Such patterns are interpreted as indicators of enzymes being present not only on the roots but also in roots' vicinity and, thus, of higher root-driven enzymatic activity in the rhizosphere. Our results indicate that such interpretations should be made with caution. In our experiment there was no soil or any other source of MUF besides the MUF-saturated roots themselves. Yet, clear spatial gradients in MUF content developed overtime as a function of the distance from the roots (Fig. 3). Both lateral and radial diffusion contributed to the observed patterns. The tails of the MUF distributions in Fig. 3, in part, were associated with the longer diffusion distances to these locations (Fig. 10, red arrows), and thus longer MUF travel time.

It is beyond doubt that biological, and hence, enzymatic activities (except for phosphatase (Giles et al., 2018; Hummel et al., 2021)) in the rhizosphere are typically higher than in the surrounding non-rhizosphere soil (Razavi et al., 2016; Kuzyakov and Razavi, 2019). Proximity

to the roots drives the high enzymatic activities by root exudation (Pausch and Kuzyakov, 2011; Holz et al., 2018), presence of root hairs (Ma et al, 2018); higher microbial density and activity, and many other biological processes. Nevertheless, it is worth making the point that quantification of the spatial patterns in enzymatic activities using the membrane zymography is rather challenging. A clear separation between the true spatial pattern of the enzyme presence and the MUF diffusion artifacts unlikely be attained.

4.2 Root zymography experiment

The results of *Root zymography experiment* clearly showed that dynamics of MUF content in the membranes were non-linear, and the slope of MUF vs. time curves constantly changed over time. The non-linear behavior introduces uncertainty into enzymatic activity calculations. Indeed, when using a single zymogram taken at different time points, the activity estimated from data in Fig. 4b ranged from 0.396 to 1.084 pmol mm^{-2} min^{-1} and from 0.082 to 0.360 pmol mm^{-2} min^{-1} for the middles of *root-2a* and *root-2b*, respectively. It is worth to note, that the peak activity was observed at 20^{th} minute of the *Root zymography experiment* on *root-2a,* while the activity on *root-2b* approached a plateau with activity of 0.360 pmol mm^{-2} min^{-1} only on the 45^{th} minute of the experiment (Fig. 4c). Ironically, the activity in *root-2a* was the smallest when the activity in *root-2b* was the highest. Using a single zymogram for either 20^{th} or 45^{th} minute incubation duration would underestimate the activity in one of the two roots. It is clear, that on zymograms of actual root-soil samples, the variations in peak activities can be much larger than those observed in just two roots used in this experiment. This implies that the results of spatial analyses of enzymatic activities obtained from a single-incubation-duration zymogram, as done in traditional 2D zymography, can be misleading, because of non-linear changes in MUF contents and because the peak activities in different locations on the membrane tend to occur at different times.

As noticed earlier in the *MUF diffusion experiment*, radial MUF diffusion from the roots to the membrane and lateral diffusion within the membrane created an illusion of enzyme activity decreasing with the distance from the root. The only source of MUF in that experiment was the MUF added to the roots, and it was, thus, the only diffusing substance. On the contrary, in the *Root zymography experiment*, it is theoretically possible that not only the produced MUF, but also the enzymes themselves diffused during the incubation (Spohn and Kuzyakov, 2013, 2014;

Holz et al., 2019; Hummel et al., 2021). The comparison of *MUF diffusion* in the *Root zymography experiments* indicated that the diffusion of the enzymes was negligible and the produced MUF was the only substance subject to appreciable diffusion. First, the shapes of MUF content dynamics in the *Root zymography experiment* were similar to those in the *MUF diffusion experiment* (Fig. 4 a,b). Enzyme diffusion would introduce oscillations to the MUF curves due to relocation of enzymes relative to the membrane surface. These oscillations are absent in Fig. 4, and the shapes of MUF content dynamics are smooth. Second, omnidirectional enzymes moving from the root would produce additional MUF diffusion front to the existing one due to relocation of MUF producers further from the root surface. In this case we would observe increasing over time tailing parts on MUF content curves (Fig. 3c,d). However, shapes of the MUF curves were even more abrupt in the *Root zymography experiment (Fig.* 3c,d) as compared to the *MUF diffusion experiment*. These observations are consistent with Guber et al. (2019) who showed experimentally that enzymes do not diffuse more than 0.1 mm, if at all, during soil zymography.

4.3 Modeling the root zymography experiments

Acceptable accuracy of HYDRUS-2D & HP2 in modeling the results of *Root zymography experiment* confirmed correctness of the model assumptions, namely, that the key processes controlling the 2D soil-membrane zymography were molecular diffusion of the substrate from the membrane to roots, cleavage of the diffused substrate by enzymes described by the concentration-dependent Michaelis-Menten equation (2), and backward diffusion of the product (MUF) to the membrane.

Modeling revealed and explained three important features of the soil membrane zymography. The first feature was the impact of the distance between the membrane and the soil/root surfaces on the length of the delay in the time of MUF appearance in the membrane (lag time). In the *Root zymography experiment* the lag time was around 20 min for *root-2a* (Fig. 4b, red circles) and close to zero in the root-associated area of *root-2b* (Fig. 4b, black circles). During simulations, adjusting the distance between the membrane and the roots enabled correct modeling of the lag time length. The lag time was close to zero in the simulations where the root surfaces were in direct contact with the membrane, i.e., distance of 0 mm (data not shown). The enzymes located in the contact area received the substrate immediately and released MUF to the membrane. However, these modeling results deviated from the experimental data for *root-2a*. An acceptable model fit for this root, with very short lag time (~ 3 min) (Fig. 5a), was achieved by

moving the root from the membrane surface to the distance of 0.08 mm, which was comparable with the thickness of the membrane. Much larger lag time for *root-2b* (Fig. 5b) was adequately reproduced by the model when the distance was increased to 0.19 mm. These results confirmed our earlier findings that rough surface of soil and roots precludes direct contacts between the membrane and the sample during 2D zymography (Guber et al., 2018). The promising finding of this study is that modeling can be used to estimate the distances between actual enzyme positions within the studied samples and the MUF appearance on the membranes based on the lag time values.

The second feature was the influence of the distance between the membrane and enzymes on dynamics of the MUF content. Modeling clearly showed that an increase in the distance between the membrane and the root not only increased the lag time but affected the shape of the MUF dynamics. Initially, we hypothesized that the dynamics of MUF content should follow a convex curve. The expectation was that, as time progresses, the downward movement of the substrate and involvement of ever-increasing number of enzymes into MUF production would lead to a continuously increasing slope of the MUF content vs. time relationship, thus, resulting in convex MUF curves. However, in the *Root zymography experiment* the MUF dynamics curve in the root-associated zone (< 0.1mm) was concave for *root-2a* (Fig. 5a, black lines) and *S*-shaped for *root-2b* (Fig. 5b, black lines). The discrepancy between our expected and observed results can be due to several reasons. First, the concentrations of the substrate diffusing downward from the membrane were much smaller than the initial substrate concentration in the membrane, and they further decreased with the distance from the membrane. Therefore, MUF production in the distant zones was controlled more by the substrate availability to enzymes, than by V_{max}. Second, our simulations clearly showed that the substrate content decreased with time in the membrane due to diffusion losses and enzymatic activity, and at a certain time its content was not sufficient to maintain the maximum enzymatic activity in close proximity to the membrane. Third, MUF losses exponentially increased with the distance from the membrane, so contributions to the membrane from the MUF produced by distant enzymes was insignificant. The modeling results are in agreement with the results of the *Root zymography experiment*, which showed larger percentages of MUF recovery on the membrane for *root-2a* as compared with *root-2b* (Fig. 6a) due to smaller distance between *root-2a* and the membrane.

The third feature observed in the experiments and explained by the model were the changes in characteristics of MUF curves in the membrane sections with increasing distance from the root centers. These changes included appearance of the lag time, changes from concave to *S*-shaped and convex curves, and a decrease in absolute values of MUF contents in the membrane with increasing distance from enzymes on root surfaces. All these changes were explained by modeling solely due to the distance between the membrane and the enzymes source without the assumption of enzyme diffusion in the membrane or solution from their original locations. Moreover, the observed features suggested the need for measurements of MUF dynamics at high time resolution during 2D zymography for their correct interpretation and estimation of enzymatic activity.

The distance between root and membrane surfaces affected MUF recovery in the membranes. Closer distance to the membrane and shorted diffusion length resulted in greater percentage of the total produced MUF appearing in the membrane for *root-2a* as compared with *root-2b* (Fig. 6a, black lines). The percentage of the total MUF produced in the whole system that approached the membrane ($100\%P^t_{detected}/P^t_{total}$) constantly increased for both roots in the simulations (Fig. 6a). The increase occurred due to decreasing total MUF production in the system (denominator P^t_{total}) as a result of decreasing substrate content in the system with time, on one hand, and simultaneous increasing cumulative influx of MUF from the solution around the roots to the membrane (numerator $P^t_{detected}$), on the other hand. Contrary to the percentage of MUF in the whole membranes, the percentage of MUF in the root-associated areas plateaued as a result of MUF losses to lateral diffusion inside the membranes (Fig. 6a, red lines). The shape of both curves indicates increasing with time dominance of MUF redistribution from enzyme active zones over MUF production within these zones.

Low MUF recovery in the membranes obtained in simulations confirmed our earlier findings that traditional soil zymography considerably underestimates enzymatic activity due to MUF losses to diffusion (Guber et al., 2018). Moreover, constantly changing percentage of recovered MUF and the differences in shapes of the recovery curves for the two roots obtained in this study imply that the results of the traditional zymography depend on the time point when the images were acquired. Our simulations showed that, due to the differences in distances between the membrane surface and enzyme positions within soil/root systems, the differences in percentage of recovered MUF for the two roots were the largest within the first 10 minutes of zymography

and then decreased with time. This can cause a wrong impression that longer zymography (i.e. 60-90 min) results in more accurate estimates of enzymatic activity. Actually, the peak activities in simulations occurred within the first 20 and 25 min of the experiment, and in the whole system and root-associated areas, respectively (Fig 6b). The time until reaching the peak activity was almost two times shorter in *root-2a* than in *root-2b*, implying that the effect of the distance on the enzyme activity calculations cannot be ignored.

The two-fold and three-fold differences in the peak activities estimated for the whole system and for the root-associated areas were much greater than could be expected from the differences in V_{max} values (67 vs. 62 nmol min^{-1} ml^{-1}) between the two roots obtained in fitting HYDRUS-2D & HP2 model to the experimental data (Fig. 5). One reason for that was much lower concentrations of the substrate available for enzymes at larger distances from the membrane in case of *root-2b*. Another reason was larger diffusion losses of MUF to the solution around this root. Indeed, the peak activities in the root-associated areas of the membranes estimated from data in Fig. 6b comprised only 3.9% and 2.7% of the total enzymatic activity in the systems for *root-2a* and *root-2b*, respectively.

Overall, modeling the *Root zymography experiment's* results clearly showed the complexity of the processes involved in the membrane soil zymography and revealed weaknesses of the traditional approach to estimating enzymatic activity. We realize that it is impractical to calibrate the model for each pixel in zymograms in order to calculate the enzymatic activity in soil/root area associated with this pixel. However, we assume that reasonable estimates for the activity can be obtained from analysis of MUF content dynamics in individual pixels using proposed TLZ.

4.4 Modeling case study: the effect of the enzyme position on soil zymography results

Modeling soil-root zymography with variable distance between the enzymes on the root surface and the membrane provided new insights into the thickness of the soil layer that can be assessed by the membrane zymography and the potentially detectable fraction of the total enzymatic activity within this layer. The highest detection capacity, i.e., from 13% to 20% of the total activity, within the range of modeled V_{max} values (10 – 100 nmol min^{-1} ml^{-1}) was possible only in case of the direct contact of the membrane with the enzymes. These numbers deviate appreciably from 100% due to MUF diffusion. The detection level dropped fast with increasing distance from the membrane, and at a distance of 40 μm reached only half of that for the perfect

contact (Fig. 7c). Further increase in the distance up to 0.2 mm resulted in only 4% detection capacity. Therefore, only 200 μm soil-root layer on contact with the membrane is essential for 2D membrane zymography, implying that, contrary to the enzyme assays in soil suspensions, the membrane-based zymography is a surface-survey method. The low detection capacity suggests, that an overall accuracy of the traditional membrane zymography is low and mostly can be used for comparison purposes. For the quantitative assessments, the results of 2D membrane zymography need to be corrected for the diffusion losses under specific experimental conditions. Moreover, since the distance between membrane and enzymes is related to the solute travel time, the activity detected at the perfect attachment drops exponentially as a function of the time to reach the peak activity (Fig. 7d). The time t_{50} (Eq.(6)), when the activity drops by half was only 3.8 min, implying that zymography must last as short as possible. Unfortunately, in practice it is rarely achievable due to rough soil and root surfaces, that typically results in a much longer lag time on zymograms.

One way to correct the results of soil zymography is using Eq.(7). The unknown variable in this equation is the time to reach peak activity, t_p, which must be calculated for each pixel of a zymogram. The radial MUF diffusion to and lateral diffusion inside the membrane produce a diffusion front, which widths in the membrane increases over time. In zymograms the diffusion front appears as image blurring, with MUF diffusion from multiple enzyme-active zones overlapped. Due to nonlinear increase of the correction factor f with t_p, the f values in the diffusion area with large t_p are greater than those in the enzyme-associated pixels, where t_p values are small. As a result, the activity calculated in the diffusion area may exceed that in the enzyme zones. This artifact must be corrected as well.

4.7 Comparing results of traditional and time-lapse zymography

Expressing the activity as a maximum time derivative of MUF detected in the membrane over zymography duration in TLZ considerably improved the histograms of the peak activities and made them more meaningful. Indeed, continuous decline of abundance of active pixels with increasing activity obtained for traditional zymography approach in all experiments (Fig. 8, top raw, closed symbols) is difficult to explain from theoretical point of view. From mathematical point of view this fact can be explained by linearization of non-linear MUF content dynamics by the traditional method. Indeed, using a single image and assuming linear growth of MUF

contents in pixels over time produces the same activity for convex and concave curves, if MUF levels at a time of image acquisition are the same in both curves. The TLZ is free of this assumption, and thus it more correctly processes the MUF time series. Theoretically, the convex and concave MUF curves (Fig. 5) may have the same values of maximum derivatives $\max(v_i^t)$. However, the activity peaks much early on the concave than on convex curves, and therefore, the same peak activity values corrected using Eq. (7) are larger for the convex than for in the concave curves. Considering, that imperfect contact between the membrane and soil surface causes the lag time in MUF appearance on the membrane (Fig. 5), the convex curves must dominate in zymograms. Therefore, the histograms for corrected images (Fig. 8, bottom row) are skewed toward large peak time t_p.

Correcting enzyme activity for MUF diffusion losses in a course of TLZ changed the shapes of data histograms from linear to bell-shaped (in lognormal scale) (Fig 8, bottom row). These histogram shapes of activity distributions are much more meaningful than linear ones obtained from the traditional zymography (Fig. 8, top row), since they adequately represent the enzyme population with contrasting activities on soil and at root surfaces.

The approach developed in this study generated less diffusive maps of enzymatic activity on root surface and in soil. Correction for MUF losses resulted in much higher activities as compared with the traditional zymography. This occurred due to fast declining percentage of activity detected in the enzyme-associated area of the membrane with the increasing peak time (Fig. 7d), and high abundance of pixels with lag time in zymograms (Fig. 8, top row) resulted in values of the correction factors of 23.5±2.5, 24.4±3.1 and 24.6±2.4 for Root, Control and Switchgrass zymograms, respectively. We realize that the coefficients of the Eq. (7) were obtained on a small dataset with well-defined enzyme locations on root surface. Moreover, size of the roots was much larger than the image resolution, resulting in overlapping MUF diffusion fronts originated from neighboring pixels on the root surface. This effect can be less expressed in fine soil fractions, that potentially decreases the percentage of detection activity and increases f values. This was likely the explanation for differences between root and soil histograms in Fig. 8 (bottom row). Therefore, these parameters must be used cautiously for soil zymography. Their estimates for different soils and soil-root systems is an interesting topic for new studies.

Theoretically, new approach allows volumetric estimates of enzyme activity. Mean and standard deviations of peak activities for the corrected zymograms were 10.0 ± 2.4 and 11.4 ±

4.1 pmol min^{-1} mm^{-2} in the control and switchgrass samples, respectively (Fig. 9, bottom row). Assuming the thickness of the surveyed layer for TLZ of 0.2 mm and soil bulk density of 1.2 g cm^{-3} the estimates for volumetric β-glucosidase activity would be 41.6 ± 10.1 and 47.6 ± 17.0 nmol min^{-1} g^{-1}. These estimates are within the range of V_{max} obtained in traditional enzyme assays for the Hallsworth series soil of UK (Marx et al., 2001) and eleven Midwestern soils of USA (Eivazi & Tabatabai, 1988). Comparison of TLZ with traditional enzyme assays were beyond objectives of this study, but it opens an interesting avenue for future research.

CONCLUSIONS

We developed time-lapse zymography (TLZ) approach as an advancement of the traditional 2D membrane zymography. It is based on: (i) nearly continuous imaging of MUF occurrence in the membrane, (ii) pixel-based calculation of the steepest gradients of MUF changes over time, (iii) estimation of the times with peak activities, and (iv) correcting the activity maps for MUF diffusion losses. By using the highest rates of signal development from linear parts of MUF dynamics in individual pixels of zymography images, TLZ resolves the problems of non-linearity in MUF content dynamics and membrane oversaturation by MUF, which plague traditional soil zymography.

Experimental and modeling results of this study do not support the assumption of enzyme diffusion during zymography. MUF dynamics in the zymography membrane can be adequately reproduced solely by: (i) diffusive transport of substrate from membrane, (ii) catalytic enzyme reaction described by the substrate concentration-dependent Michaelis-Menten equation, and (iii) diffusion of the product to the membrane.

While the new approach developed in this study provides more accurate estimates of enzyme activity, it does not resolve all issues of traditional single-image zymography. TLZ still requires a standardization for different soils and enzyme types, a better separation of MUF amounts diffused to the membrane from multiple hotspots, and improvements in handing imperfect contacts between soil/roots and membranes.

Combining TLZ with modeling revealed a high potential of the new approach for future development of membrane zymography in soil applications. Particularly promising future directions are (i) defining optimal concentrations of substrate and zymography duration for

different soils and enzymes; (ii) linking surface zymography with microplate fluorimetric assays; and (iii) obtaining volumetric (3D) estimates of enzyme activity at larger spatial scales.

ACKNOWLEDGEMENT

Support for this research was provided in part by the NSF DEB Program (Award # 1904267), by the NSF LTER Program (DEB 1027253) at the Kellogg Biological Station, by the Great Lakes Bioenergy Research Center, U.S. Department of Energy, Office of Science, Office of Biological and Environmental Research under Award Number DE-SC0018409, by the German Research Foundation (DFG; project number 403664478) in context of Priority Programme 2089 "Rhizosphere spatiotemporal organization", the "RUDN University program 5-100" and Russian Science Foundation (project No. 18-14-00362).

Appendix A. Supplementary data Supplementary data to this article can be found online at https://doi.org/10.1016/j.soilbio.2021.108225.

DECLARATION OF INTERESTS

The authors declare that they have no known competing financial interests or personal relationships that could have appeared to influence the work reported in this paper.

REFERENCES

Allison, S.D., Wallenstein, M.D., Bradford, M.A., 2010. Soil-carbon response to warming dependent on microbial physiology. Nature Geoscience 3, 336–340.

Baldrian, P., Větrovský, T., 2012. Scaling down the analysis of environmental processes: Monitoring: Enzyme activity in natural substrates on a millimeter: Resolution scale. Applied and Environmental Microbiology 78(9), 3473–3475. doi.org/10.1128/AEM.07953-11.

Buades, A., Coll, B., Morel, J-M., 2011. Non-local means denoising. Image Processing On Line 1, 208–212. http://dx.doi.org/10.5201/ipol.2011.bcm.

Darbon, J., Cunha, A., Chan, T., Osher, S., Jensen, G., 2008. Fast nonlocal filtering applied to electron cryomicroscopy. In: 2008 5th IEEE International Symposium on Biomedical Imaging: From Nano to Macro, Proceedings, ISBI. IEEE, 1331–1334.

Dinkelaker, B., Marschner, H., 1992. In vivo demonstration of acid phosphatase activity in the rhizosphere of soil-grown plants. Plant Soil 144: 199-205. doi.org/10.1007/BF00012876.

Dong, S., Brooks, D., Jones, M.D., Grayston, S. J. 2007. A method for linking in situ activities of hydrolytic enzymes to associated organisms in forest soils. Soil Biology and Biochemistry, 39(9), 2414–2419. doi.org/10.1016/j.soilbio.2007.03.030.

Eivazi, F., Tabatabai, M.A.,1988. Glucosidases and galactosidases in soils. Soil Biology and Biochemistry 20(5), 601–606. https://doi.org/10.1016/0038-0717(88)90141-1

Ge, T., Wei, X., Razavi, B.S., Zhu, Z., Hu, Y., Kuzyakov, Y., Jones, D.L., Wu, J., 2017. Stability and dynamics of enzyme activity patterns in the rice rhizosphere: Effects of plant growth and temperature. Soil Biology and Biochemistry 113, 108–115. doi:10.1016/j.soilbio.2017.06.005

German, D.P., Marcelo, K.R.B., Stone, M.M., Allison, S.D., 2012. The Michaelis–Menten kinetics of soil extracellular enzymes in response to temperature: a cross-latitudinal study. Global Change Biology 18: 1468-1479. doi:10.1111/j.1365-2486.2011.02615.x.

German, D. P., Weintraub, M. N., Grandy, A. S., Lauber, C. L., Rinkes, Z. L., Allison, S. D. 2011. Optimization of hydrolytic and oxidative enzyme methods for ecosystem studies. Soil Biology and Biochemistry 43(7), 1387–1397. https://doi.org/10.1016/j.soilbio.2011.03.017

Giles, C.D., Dupuy, L., Boitt, G., Brown, L.K., Condron, L.M., Darch, T., Blackwell, M.S.A., Menezes-Blackburn, D., Shand, C.A., Stutter, M.I., Lumsdon, D.G., Wendler, R., Cooper, P., Wearing, C., Zhang, H., Haygarth, P.M., T.S. George, 2018. Root development impacts on the distribution of phosphatase activity: Improvements in quantification using soil zymography, Soil Biology and Biochemistry 116, 158-166. https://doi.org/10.1016/j.soilbio.2017.08.011

Grierson, P.F., Comerford, N.B., 2000. Non-destructive measurement of acid phosphatase activity in the rhizosphere using nitrocellulose membranes and image analysis. Plant and Soil 218, 49–57.

Guber, A., Kravchenko, A., Razavi, B., Uteau, D., Peth, S., Blagodatskaya, E., Kuzyakov, Y., 2018. Quantitative soil zymography: Mechanisms, processes of substrate and enzyme diffusion in porous media. Soil Biology and Biochemistry 127: 156-167.

Guber, A.K., Kravchenko, A.N., Razavi, B.S., Blagodatskaya, E., Kuzyakov, Y. 2019. Calibration of 2-D soil zymography for correct analysis of enzyme distribution. European Journal of Soil Science 70(4): 715-726.

Guhr, A., Borken, W., Spohn, M., Matzner, E., 2015. Redistribution of soil water by a saprotrophic fungus enhances carbon mineralization. Proc. Natl. Acad. Sci. Unit. States Am. 112, 14647–14651.

Heitkötter, J., Marschner, B., 2018. Soil zymography as a powerful tool for exploring hotspots and substrate limitation in undisturbed subsoil. Soil Biology and Biochemistry 124, 210–217.

Hoang, D.T.T., Razavi, B.S., Kuzyakov, Y., Blagodatskaya, E., 2016. Earthworm burrows: Kinetics and spatial distribution of enzymes of C-, N- and P- cycles. Soil Biology and Biochemistry 99, 94–103. doi:10.1016/j.soilbio.2016.04.021.

Holz, M., Zarebanadkouki, M., Carminati, A., Hovind, J., Kaestner, A., Spohn, M., 2019. Increased water retention in the rhizosphere allows for high phosphatase activity in drying soil. Plant and Soil 443(1–2), 259–271. https://doi.org/10.1007/s11104-019-04234-3

Holz, M., Zarebanadkouki, M., Kuzyakov,Y., Pausch, J., Carminati, A., 2018. Root hairs increase rhizosphere extension and carbon input to soil. Annals of Botany 121(1), 61–69. https://doi.org/10.1093/aob/mcx127

Hummel, C., Boitt, G., Santner, J., Lehto, N.J., Condron, L., Wenzel, W.W., 2021. Co-occurring increased phosphatase activity and labile P depletion in the rhizosphere of *Lupinus angustifolius* assessed with a novel, combined 2D-imaging approach. Soil Biology and Biochemistry 153, 107963. https://doi.org/10.1016/j.soilbio.2020.107963.

Johnson, K., Goody, R., 2011. The Original Michaelis Constant. Biochemistry 50, 39, 8264–8269. doi:10.1021/bi201284u.

Jones, M.D., Brooks, D.D., Courty, P., Garbaye, J., Grierson, P.F., 2011. Methods of soil enzymology enzyme activities of root tips and in situ profiles of soils and rhizospheres. In: Dick R.P. (Ed). Methods of soil enzymology, pp. 275-309, Soil Science Society of America, Inc., Book series 9, Madisom, Wisconsin, USA. doi: 10.2136/sssabookser9.c13.

Kuzyakov, Y., Razavi, B.S., 2019. Rhizosphere size and shape: Temporal dynamics and spatial stationarity. Soil Biology and Biochemistry 135, 343-360. https://doi.org/10.1016/ j.soilbio.2019.05.011.

Linton, W.H., Sherwood, T.K., 1950. Mass Transfer from Solid Shapes to Water in Streamline and Turbulent Flow, Chemical Engineering Progress 46(5), 258-264.

Liu, S., Razavi, B.S., Su, X., Maharjan, M., Zarebanadkouki, M., Blagodatskaya, E., Kuzyakov, Y., 2017. Spatio-temporal patterns of enzyme activities after manure application reflect mechanisms of niche differentiation between plants and microorganisms. Soil Biology and Biochemistry 112, 100–109. doi:10.1016/j.soilbio.2017.05.006.

Ma, X., Razavi, B.S., Holz, M., Blagodatskaya, E., Kuzyakov, Y., 2017. Warming increases hotspot areas of enzyme activity and shortens the duration of hot moments in the root-detritusphere. Soil Biology and Biochemistry 107, 226–233.

Ma, X., Zarebanadkouki, M., Kuzyakov, Y., Blagodatskaya, E., Pausch, J., Razavi, B.S., 2018. Spatial patterns of enzyme activities in the rhizosphere: Effects of root hairs and root radius. Soil Biology and Biochemistry 118, 69–78.

Marx, M.C., Wood, M., Jarvis, S.C., 2001. A microplate fluorimetric assay for the study of enzyme diversity in soils. Soil Biology and Biochemistry, 33(12–13), 1633–1640. https://doi.org/10.1016/S0038-0717(01)00079-7

Michaelis, L., Menten, M.L., 1913. Die Kinetik der Invertinwirkung. Biochem Z 49, 333– 369.

Moriasi, D. N., Arnold, J. G., Van Liew, M. W., Bingner, R. L., Harmel, R. D., Veith, T. L., 2007. Model Evaluation Guidelines for Systematic Quantification of Accuracy in Watershed Simulations. Transactions of the ASABE 50 (3): 885–900. doi:10.13031/2013.23153.

Moyle, M.P., Tyner, M., 1953. Solubility and Diffusivity of 2- Naphtol in Water, Industrial & Engineering Chemistry Research 45(8), 1794-1797.

Pausch, J., and Kuzyakov, Y., 2011. Photoassimilate allocation and dynamics of hotspots in roots visualized by 14C phosphor imaging. Plant Nutrition and Soil Science 174 (1), 12-19.

Press, W.H., Teukolsky, S.A., Vetterling, W.T., Flannery, B.P., 2007. Section 10.2. Golden Section Search in One Dimension, Numerical Recipes: The Art of Scientific Computing (3rd ed.), New York: Cambridge University Press, ISBN 978-0-521-88068-8

Razavi, B.S., Hoang, D., Kuzyakov, Y., 2017. Visualization of Enzyme Activities in Earthworm Biopores by In Situ Soil Zymography. In: Wilkesman J., Kurz L. (Eds), Zymography. Methods in Molecular Biology, vol. 1626. Humana Press, New York, NY 10013, U.S.A.

Razavi, B., Zhang, X., Bilyera, N., Guber, A., Zarebanadkouki, M. 2019. Soil zymography: Simple and reliable? Review of current knowledge and optimization of the method. Rhizosphere 11, 100161.

Razavi, B.S., Zarebanadkouki, M., Blagodatskaya, E., Kuzyakov, Y., 2016. Rhizosphere shape of lentil and maize: Spatial distribution of enzyme activities. Environmental Modelling and Software 79, 229–237. doi:10.1016/j.soilbio.2016.02.020.

Ritter, A., Muñoz-Carpena, R., 2013. Performance evaluation of hydrological models: statistical significance for reducing subjectivity in goodness-of-fit assessments. Journal of Hydrology 480 (1): 33–45. doi:10.1016/j.jhydrol.2012.12.004.

Sanaullah, M., Razavi, B.S., Blagodatskaya, E., Kuzyakov, Y., 2016. Spatial distribution and catalytic mechanisms of β-glucosidase activity at the root-soil interface. Biology and Fertility of Soils 52, 505–514. doi:10.1007/s00374-016-1094-8.

Schindelin, J., Arganda-Carreras, I., Frise, E., Kaynig, V., Longair, M., Pietzsch, T., Preibisch, S., Rueden, C., Saalfeld, S., Schmid, B., Tinevez, J.Y., White, D.J., Hartenstein, V., Eliceiri, K., Tomancak, P., Cardona, A., 2012. Fiji: an open-source platform for biological-image analysis. Nature Methods 97: 676-682. doi: 10.1038/nmeth.2019.

Šimůnek, J., Jacques, D., Šejna, M., van Genuchten, M.Th., 2012. The HP2 Program for HYDRUS (2D/3D), A Coupled Code for Simulating Two-Dimensional Variably-Saturated Water Flow, Head Transport, Solute Transport and Biogeochemistry in Porous Media, (HYDRUS + PHREEQC + 2D), Version 1.0, PC Progress, Prague, Czech Republic, 76 pp.

Spohn, M., Carminati, A., Kuzyakov, Y., 2013. Soil zymography - A novel in situ method for mapping distribution of enzyme activity in soil. Soil Biology and Biochemistry 58, 275–280. doi:10.1016/j.soilbio.2012.12.004

Spohn, M., Kuzyakov, Y. 2013. Distribution of microbial- and root-derived phosphatase activities in the rhizosphere depending on P availability and C allocation - Coupling soil zymography with 14C imaging. Soil Biology and Biochemistry, 67, 106–113. https://doi.org/10.1016/j.soilbio.2013.08.015

Spohn, M., Kuzyakov, Y., 2014. Spatial and temporal dynamics of hotspots of enzyme activity in soil as affected by living and dead roots-a soil zymography analysis. Plant and Soil 379, 67–77. doi:10.1007/s11104-014-2041-9

Wei, X., Razavi, B.S., Yajun Hu, Y., Shen, J., Wu, J., Ge, T., 2019. C/P stoichiometry of dying rice root defines the spatial distribution and dynamics of enzyme activities in root-detritusphere. Biology and Fertility of Soils 55, 251–263.

Zhang, X., Dippold, M.A., Kuzyakov, Y., Razavi, B.S., 2019. Spatial pattern of enzyme activities depends on root exudate composition. Soil Biology and Biochemistry 133, 83–93.

Table 1. The Root-Mean-Square Errors (RMSEs) and the Nash–Sutcliffe model efficiency coefficients (NSE) for modeling MUF dynamics in the two experiments

Block	Distance from the root center	Root-2a		Root-2b	
	mm	RMSE pmol mm^{-1}	NSE -	RMSE pmol mm^{-1}	NSE -
1	0 - 0.1	0.150	0.983	0.070	0.989
2	0.10 - 0.25	0.119	0.996	0.310	0.917
3	0.25 - 0.40	0.161	0.990	0.100	0.987
4	0.40 - 0.55	0.218	0.967	0.112	0.967
5	0.55 - 0.70	0.114	0.980	0.066	0.969
6	0.70 - 0.85	0.105	0.958	0.160	0.512
Average ± Standard deviation		0.145 ± 0.042	0.979 ± 0.014	0.136 ± 0.092	0.890 ± 0.187

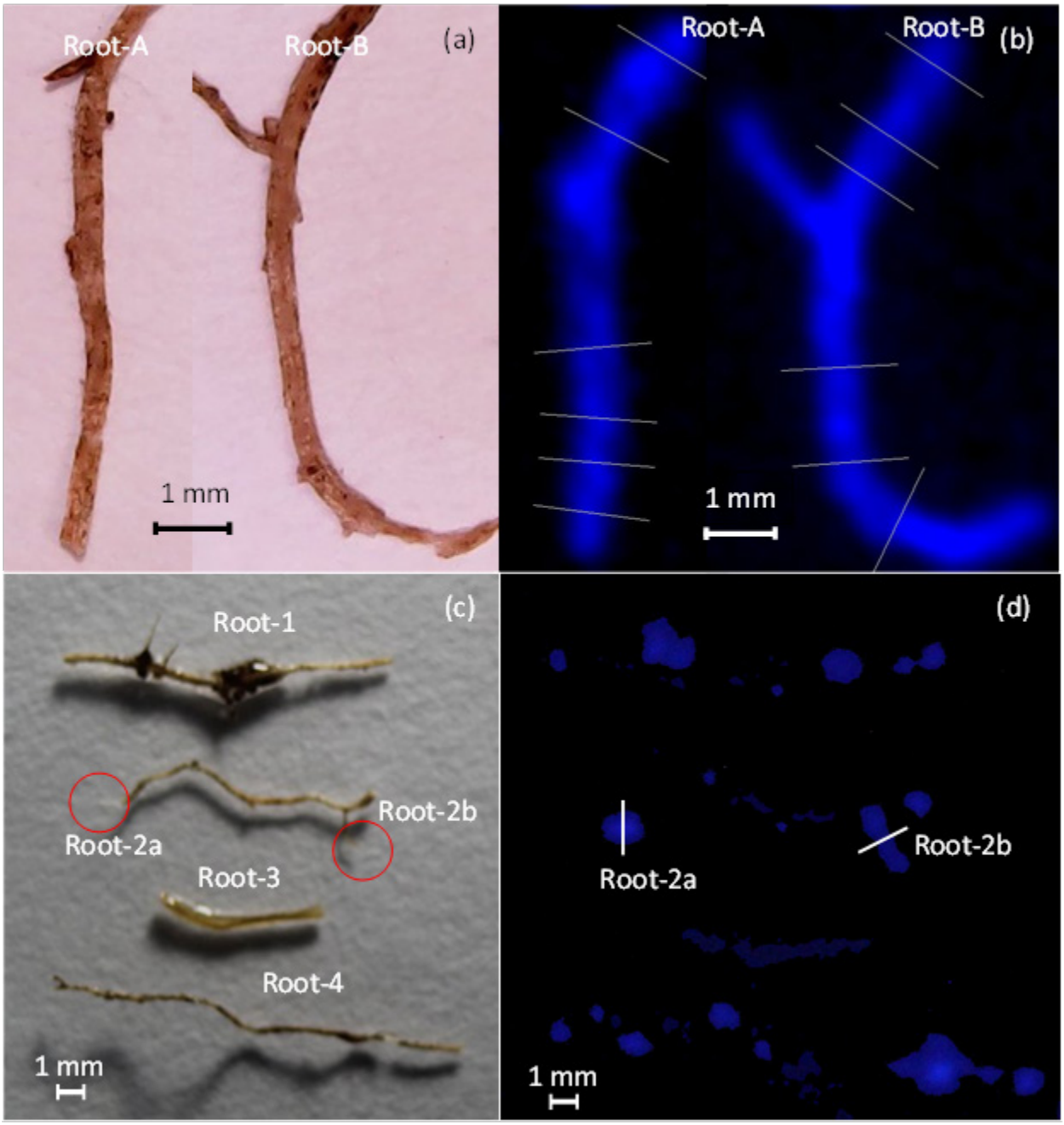

Figure 1. *MUF diffusion experiment* (top): Maize roots after saturation in 6 mM MUF solution (a), and zymographic images of the membrane after 30-min incubation on the surface of the roots (b). *Root zymography experiment* (bottom): Maize roots after saturation in DI water (c), and zymographic images of the membrane after 60-min incubation on the surface of the roots (d). White lines on (b) and (d) images show cross-sections selected for the MUF diffusion analysis and HYDRUS-2D & HP2 modeling, respectively. The background was removed and brightness of the zymograms was enhanced for presentation clarity. Red circles (c) mark the root tips used in the MUF diffusion analysis and modeling.

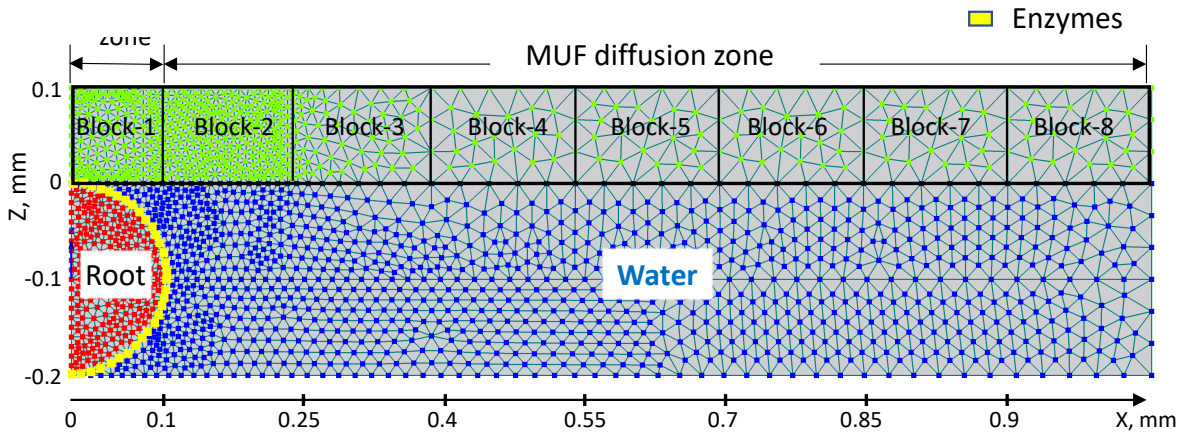

Figure 2. Mesh and material distributions for HYDRUS-2D & HP2 modeling. The colors in mesh nodes mark the membrane (green), water (blue), root (red), and enzymes on the root surface (yellow). MUF dynamics were measured in blocks 1-8 in the root zymography experiment.

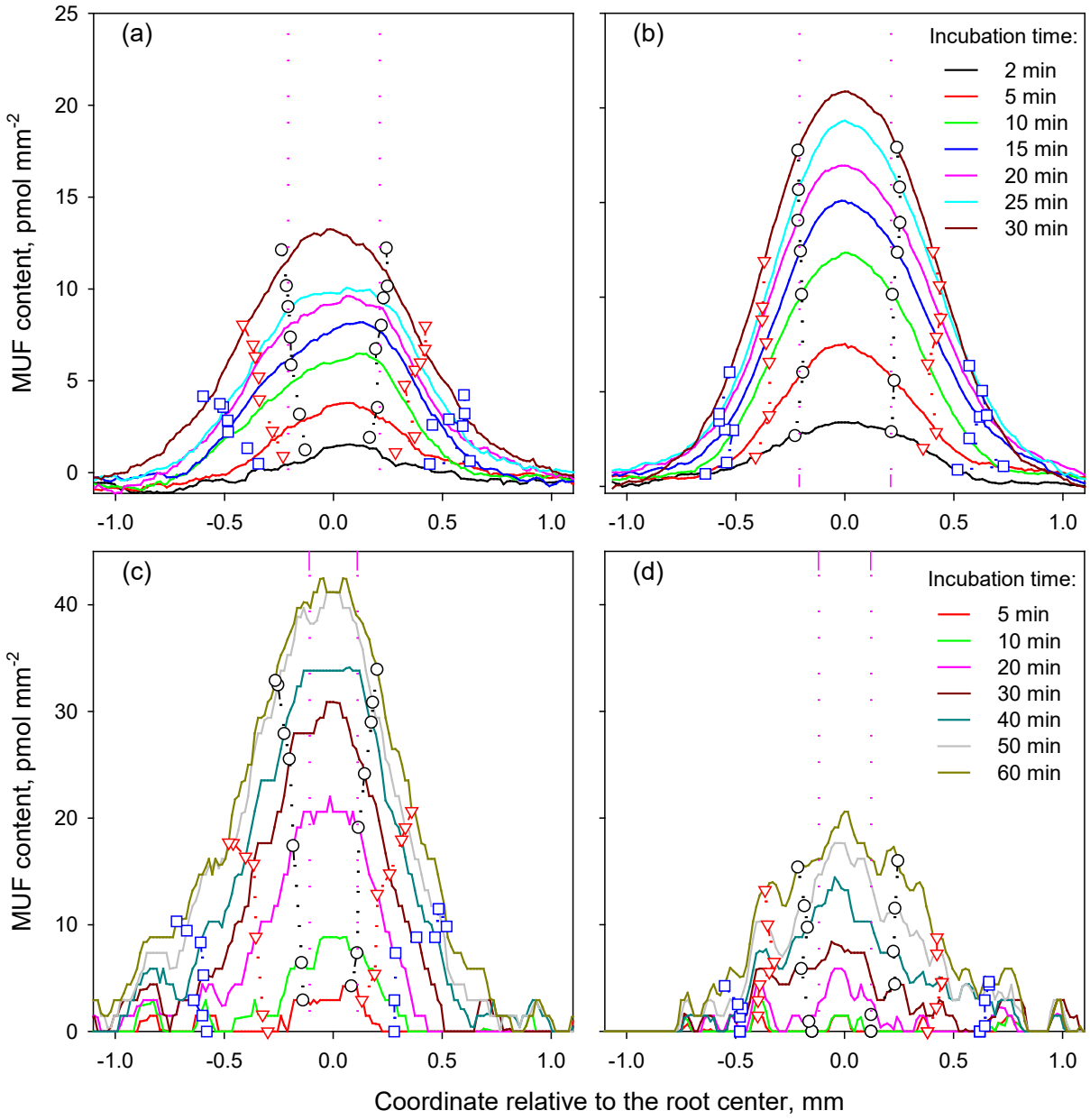

Figure 3. Distributions of MUF contents along the membrane cross-sections shown in Fig. 1b for *Root-A* (a) and *Root-B* (b) in the *MUF diffusion experiment*, and in cross-sections shown in Fig. 1d for the *root-2a* tip (c) and *root-2b* tip (d) in the *Root zymography experiment.* Pink dashed vertical lines encompass root locations. Symbols ○, △, and □ with dashed lines encompass 50%, 75% and 90 % of total MUF mass in the cross-section for each time moment, respectively. Only approximately 50% of MUF was detected in the membranes within the root areas. Another 50% of MUF diffused out of root zones.

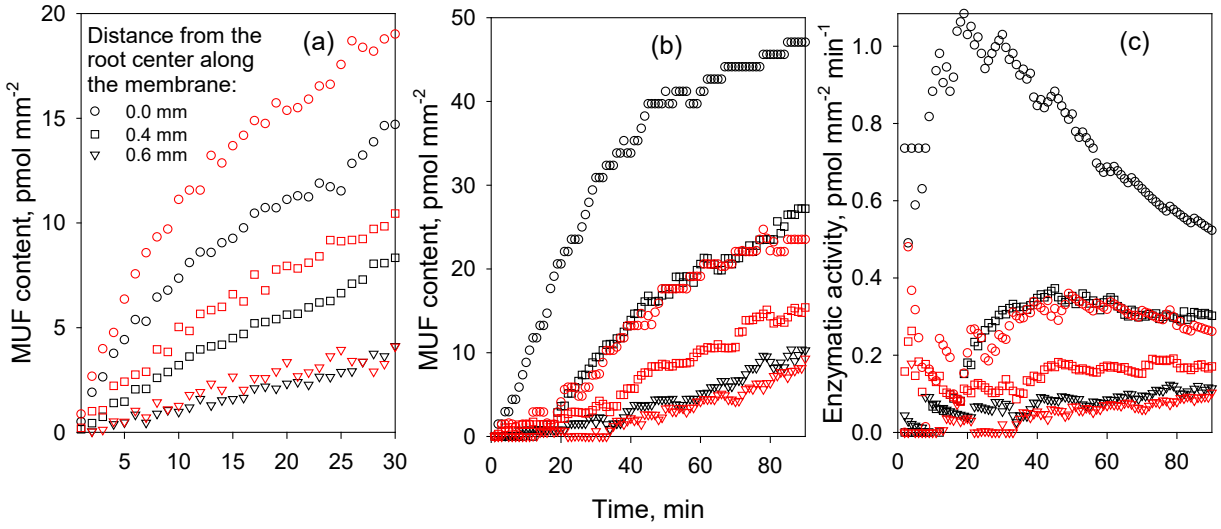

Figure 4. Time series of MUF diffused from *root-A* and *root-B* to the membrane in the *MUF diffusion experiment* (a) from *root-2a* and *root-2b* in the *Root zymography experiment* (b) detected at different distances from the root centers; and the enzymatic activity calculated from the *Root zymography experiment* time series (c). Black symbols on (a) and (b) denote the *root-A* and *root-2a*, while red symbols denote the *root-B* and *root-2b*, respectively. Black and red symbols on (c) denote the *root-2a* and *root-2*b, respectively.

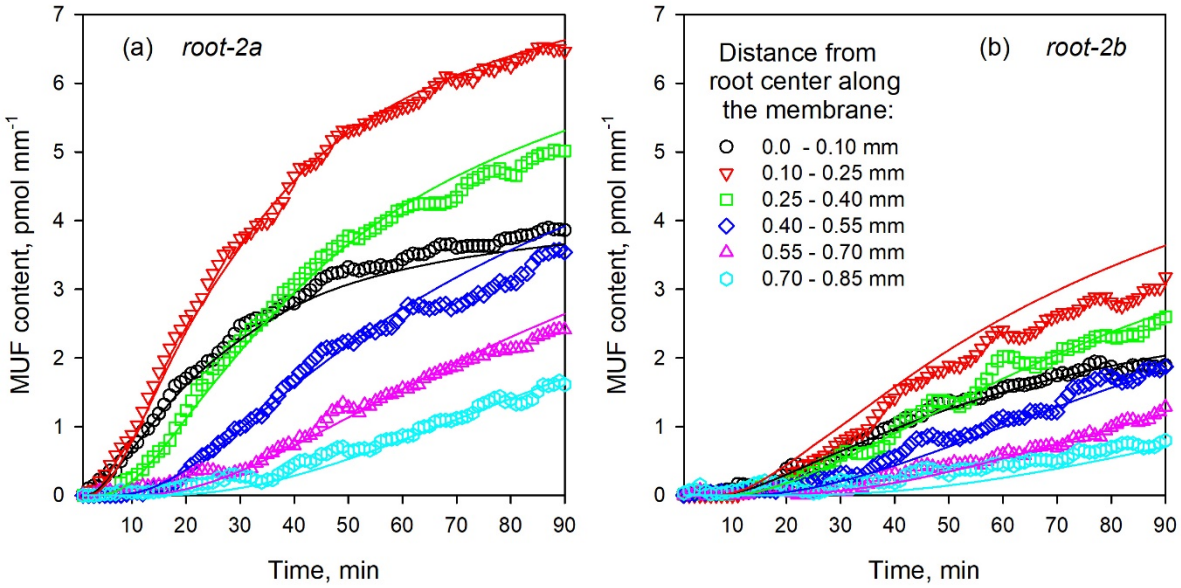

Figure 5. Model fit (lines) to the MUF contents (symbols) measured in the *Root zymography experiment* for the *root-2a* (a) and *root-2b* (b). The MUF contents are shown for blocks at different distances from centers of the roots (Fig. 2a) and expressed per unit of block width.

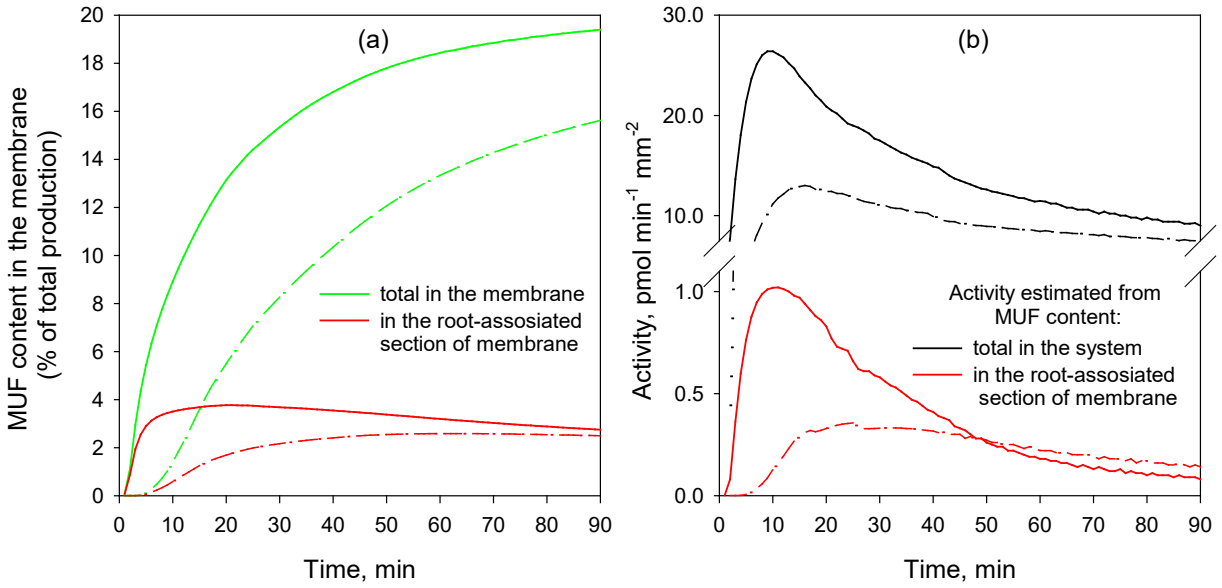

Figure 6. MUF content in the whole membrane and in the root-associated areas expressed as a percentage of the total MUF production (a), and the enzyme activity calculated using simulated values of the total MUF production in the system and in the root-associated areas of the membrane (b) for the *root-2a* (solid lines) and *root-2b* (dashed lines).

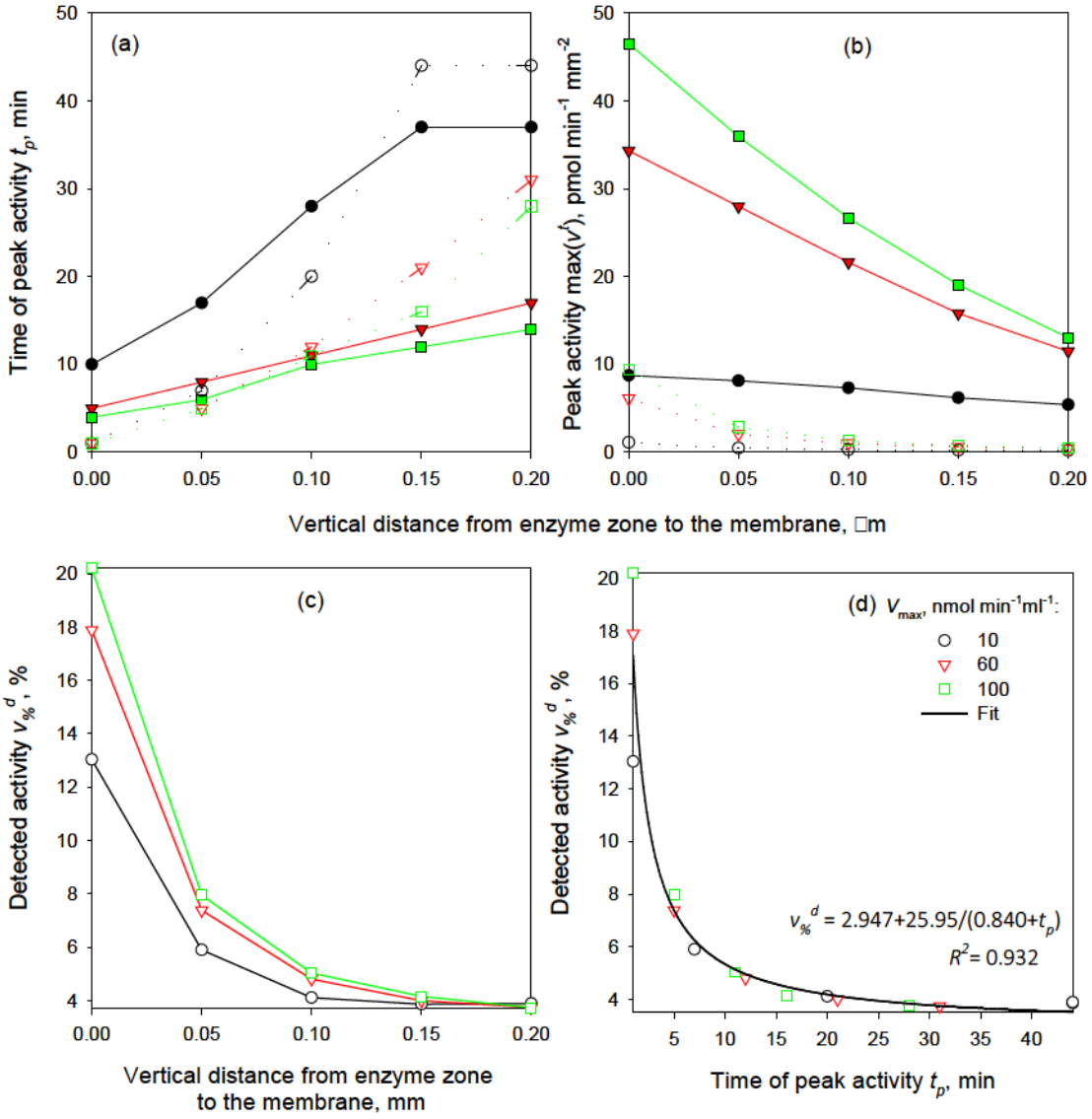

Figure 7. Times of peak enzymatic activities (a) and peak enzymatic activities (b) in the whole system (closed symbols) and in the root-associated section of the membrane (open symbols) obtained in the HYDRUS-2D & HP2 simulations at different distances from the membrane; (c) percentage of the enzyme activity detected in the root-associated section of the membrane; and (d) the detected activity as a function of the peak activity time computed from the data reported in (a) and (b) plots for the three V_{max} values.

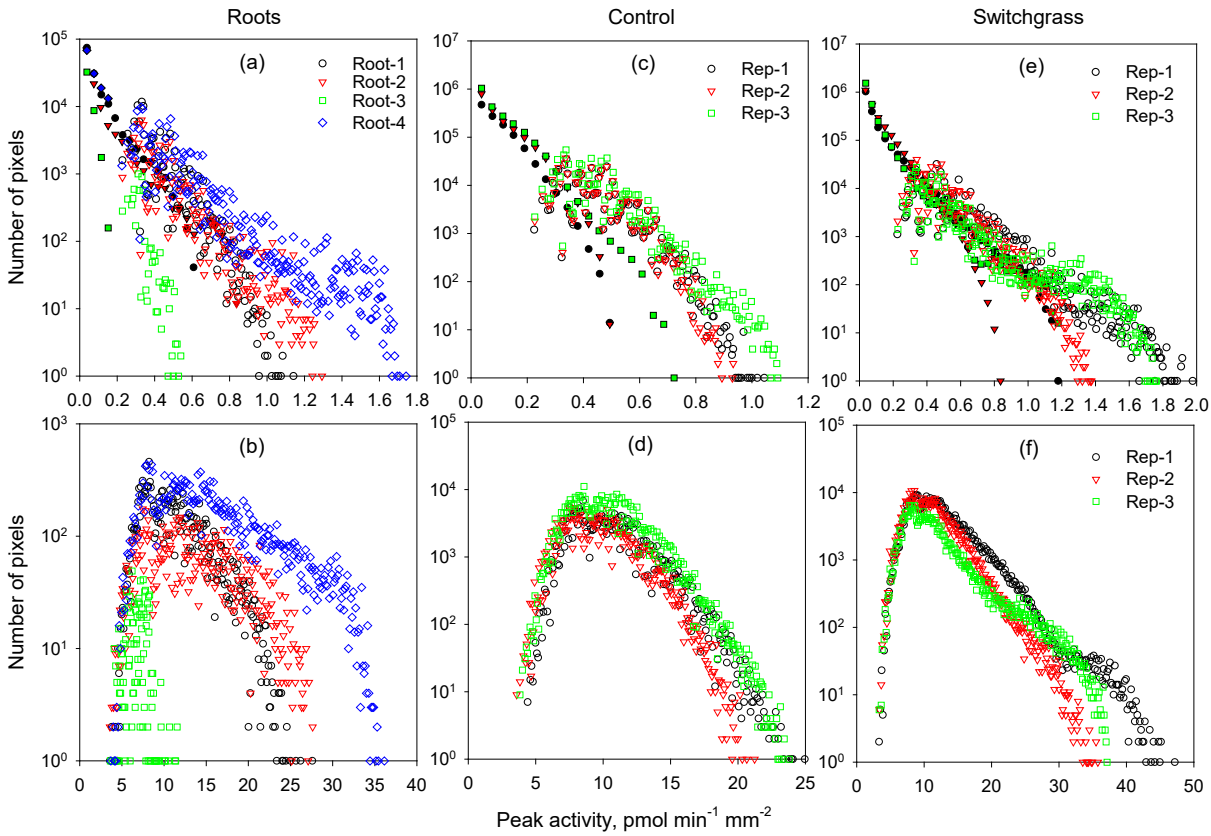

Figure 8. Histograms of enzymatic activity calculated using the traditional approach (closed symbols in the top row), and the laps time zymography before (open symbols in the top row) and after correction (bottom row).

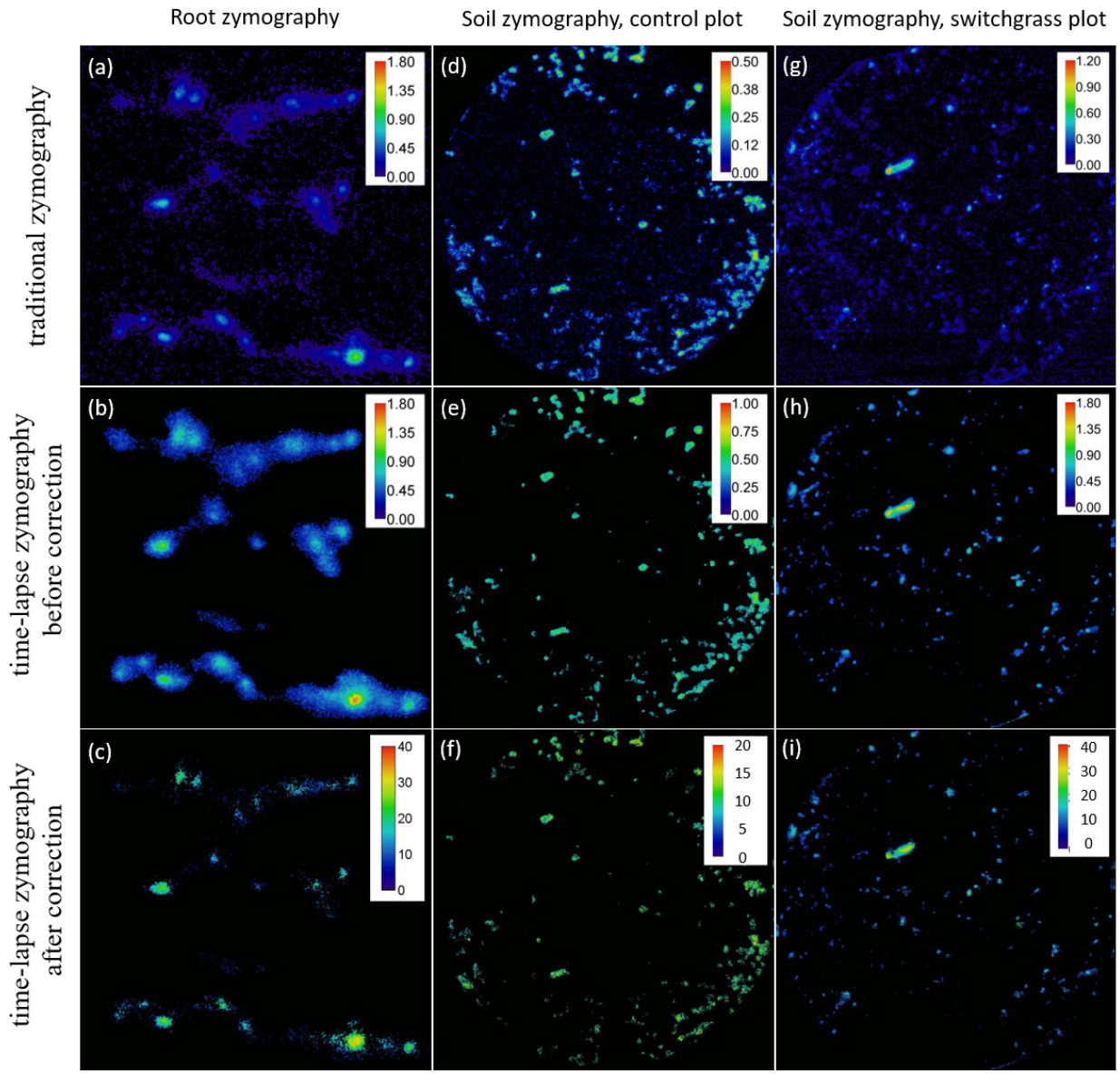

Figure 9. Examples of enzymatic activity maps computed for the *Root zymography experiment* and for the soil cores in the control (no plants) and switchgrass treatments using the traditional and time-lapse zymography. The color bars indicate the β-glucosidase activity in pmol min^{-1} mm^{-2}.

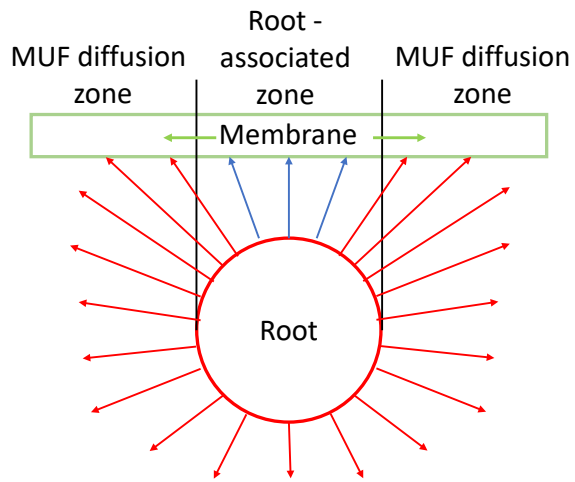

Figure 10. Schematic representation of MUF diffusion pathways in the *MUF diffusion experiment*. The color arrows indicate direct diffusion from the root to the root-associated zone on the membrane (blue), lateral diffusion within the membrane (green), and radial diffusion (red) components.

Supplemental materials

This section describes experimental setup (Fig. S1) and flowchart (Fig. S2) for time-lapse zymography.

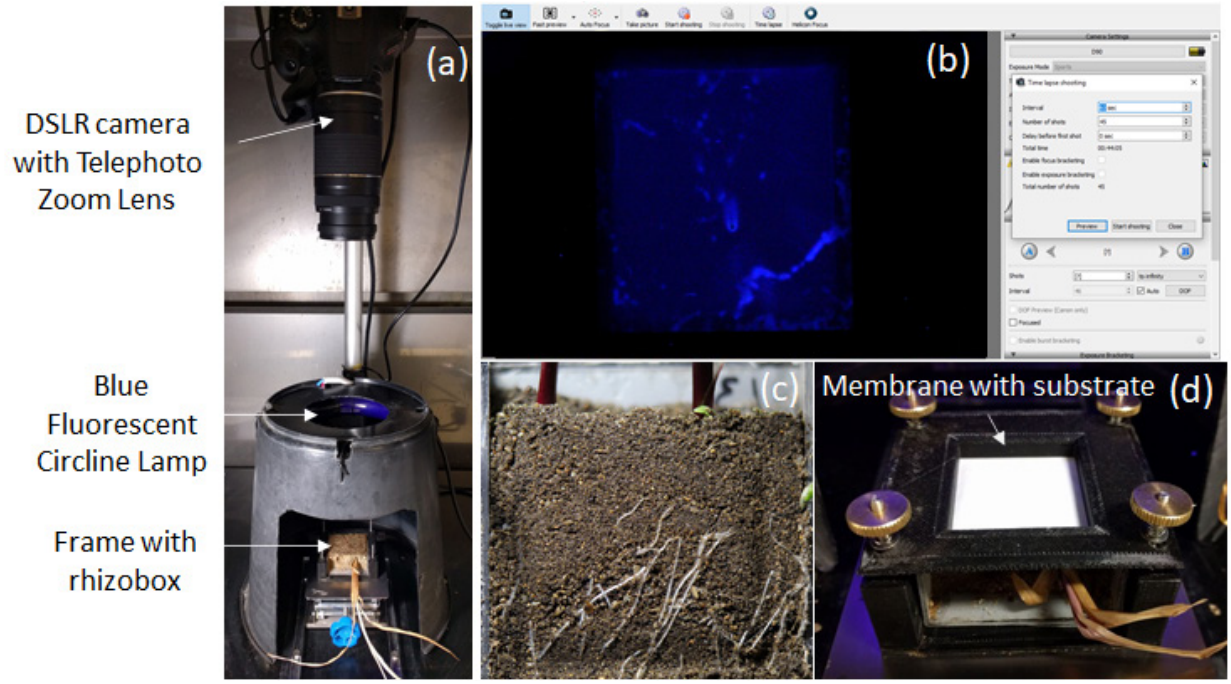

Figure S1. Experimental setup for TLZ.

S1: Experimental setup and steps of soil zymography

S1-1. The TLZ setup includes:*

1. DSLR camera
2. Telephoto Zoom Lens
3. Extension tube ring
4. Photocopy stand
5. Blue fluorescent circline lamp
6. Frame for rhizobox zymography
7. Helicon remote software

* Please see the specifications for TLZ parts used in our study in section *2.1.1* of the manuscript.

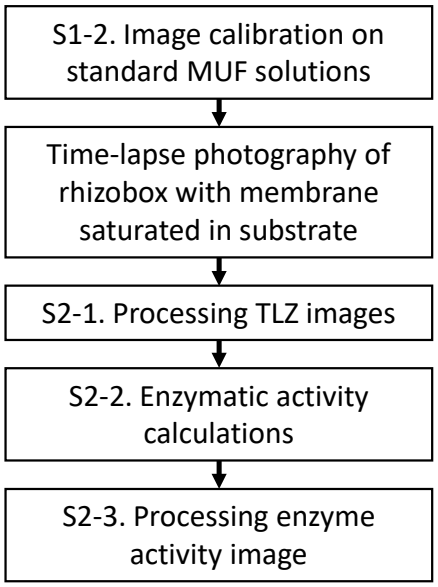

Figure S2. Flowchart for TLZ

S1-2. Image calibration on standard MUF solutions

1. Prepare MUF solutions of 0.01, 0.02, 0.04, 0.05, and 0.1mM.

2. Apply 50 µl of each concentration solution to 1 × 1 cm membranes (same as the ones used for TLZ) in 3 replications.
3. Cover membranes immediately after MUF application with a transparent film and take photos using the same settings as for TLZ.
4. Convert RGB calibration images to 8-bit greyscale images.
5. Calculate greyscale histogram for the application area at each membrane.
6. Fit the histogram to the MUF contents in the membranes using a piecewise linear regression (Guber et al., 2019).
7. Use the calibration parameters in the enzymatic activity calculation described below.

S2: Processing time-lapse zymography images.

S2-1. Processing TLZ images (ImageJ/Fiji macros)

1. Crop raw zymograms to reduce the number of processed pixels.
2. Convert RGB images into 8-bit format (without rescaling) for mathematical calculations.
3. Subtract the image taken at the start of the incubation from the whole stack of zymography images for subsequent background correction.
4. Remove the image noise with a 3D median filter (radius = 3 pixels) or a non-local means filter (Darbon et al., 2008; Buades et al., 2011) with the default settings (Sigma = 15, Smoothing Factor = 1).

S2-2. The enzymatic activity calculation (MATLAB code)

1. Convert the greyscale values in the pre-processed images to MUF content matrices using the coefficients, obtained for membrane calibration.
2. Calculate the time derivatives of MUF contents for each pixel of the membrane based on the whole images sequence using the sliding window algorithm with the desired time interval.
3. Select the largest MUF derivatives with a user-defined R^2 in each image pixel (peak activities, $v_p = \max(v_i^t)$) and save their values along with the corresponding time moments (peak activity time, t_p) as a text image files for postprocessing.
4. Calculate the correction factor *f* for the peak activities in each pixel to account for MUF losses to diffusion using the peak activity time and save it as a text image file for postprocessing.

5. Calculate and plot the statistics of calculated enzymatic activities, including: (i) total numbers of pixels (N_{pix}) with non-zero activities ($v_p > 0$) for each time moment of the zymography experiment, and (ii) the relationship between averaged enzymatic activities $\overline{v_p}$ at peak activity time moments (t_p) and these time moments.

S2-3. Processing the enzyme activity image (ImageJ/Fiji macros)

1. Select the upper and lower thresholds on $N_{pix}(t_p)$ plot for removing the noise and artifacts from the peak activity image.
2. Apply the thresholds to the peak activity time image and convert the result to a mask.
3. Apply the mask to the peak activity image and multiply the result by the image correction factor *f*.
4. Apply a color scale (Lookup Tables tool) to the 32-bit greyscale image and save it in RGB format for presentations.

** Image processing Fiji macros, MATLAB code and executable module for calibration are available from the corresponding author upon request.*